Arteriosclerosis, Thrombosis, and Vascular Biology

ORIGINAL RESEARCH

Long Noncoding RNA TPRG1-AS1 Suppresses Migration of Vascular Smooth Muscle Cells and Attenuates Atherogenesis via Interacting With MYH9 Protein

Xiaoxiao Ren, Huijuan Zhu, Keyong Deng, Xiaotong Ning, Lin Li, Dan Liu, Bin Yang, Chenyang Shen, Xianqiang Wang, Naqiong Wu, Shufeng Chen, Dongfeng Gu, Laiyuan Wang

BACKGROUND: Migration of human aortic smooth muscle cells (HASMCs) contributes to the pathogenesis of atherosclerosis. This study aims to functionally characterize long noncoding RNA TPRG1-AS1 (tumor protein p63 regulated 1, antisense 1) in HASMCs and reveal the underlying mechanism of TPRG1-AS1 in HASMCs migration, neointima formation, and subsequent atherosclerosis.

METHODS: The expression of TPRG1-AS1 in atherosclerotic plaques was verified a series of in silico analysis and quantitative real-time polymerase chain reaction analysis. Northern blot, rapid amplification of cDNA ends and Sanger sequencing were used to determine its full length. In vitro transcription-translation assay was used to investigate the protein-coding capacity of TPRG1-AS1. RNA fluorescent in situ hybridization was used to confirm its subcellular localization. Loss- and gain-of-function studies were used to investigate the function of TPRG1-AS1. Furthermore, the effect of TPRG1-AS1 on the pathological response was evaluated in carotid balloon injury model, wire injury model, and atherosclerosis model, respectively.

RESULTS: TPRG1-AS1 was significantly increased in atherosclerotic plaques. TPRG1-AS1 did not encode any proteins and its full length was 1279nt, which was *bona fide* a long noncoding RNA. TPRG1-AS1 was mainly localized in cytoplasmic and perinuclear regions in HASMCs. TPRG1-AS1 directly interacted with MYH9 (myosin heavy chain 9) protein in HASMCs, promoted MYH9 protein degradation through the proteasome pathway, hindered F-actin stress fiber formation, and finally inhibited HASMCs migration. Vascular smooth muscle cell-specific transgenic overexpression of TPRG1-AS1 significantly reduced neointima formation, and attenuated atherosclerosis in apolipoprotein E knockout ($Apoe^{-/-}$) mice.

CONCLUSIONS: This study demonstrated that TPRG1-AS1 inhibited HASMCs migration through interacting with MYH9 protein and consequently suppressed neointima formation and atherosclerosis.

Key Words: atherosclerosis ■ human aortic smooth muscle cells ■ migration ■ neointima ■ transgenic mice

Correspondence to: Laiyuan Wang, Key Laboratory of Cardiovascular Epidemiology & Department of Epidemiology, State Key Laboratory of Cardiovascular Disease, Fuwai Hospital, National Center for Cardiovascular Diseases, Chinese Academy of Medical Sciences and Peking Union Medical College, 167 Beilishi Rd, Beijing 100037, China, Email wanglaiyuandw@163.com; or Dongfeng Gu, Key Laboratory of Cardiovascular Epidemiology & Department of Epidemiology, State Key Laboratory of Cardiovascular Disease, Fuwai Hospital, National Center for Cardiovascular Diseases, Chinese Academy of Medical Sciences and Peking Union Medical College, 167 Beilishi Rd, Beijing 100037, China, Email gudongfeng@cashq.ac.cn
*X. Ren and H. Zhu contributed equally.
Supplemental Material is available at https://www.ahajournals.org/doi/suppl/10.1161/ATVBAHA.122.318158.
For Sources of Funding and Disclosures, see page XXX.

Arterioscler Thromb Vasc Biol is available at www.ahajournals.org/journal/atvb

Nonstandard Abbreviations and Acronyms

CAD	coronary artery disease
HASMC	human aortic smooth muscle cell
lncRNA	long noncoding RNA
MASMC	murine aortic smooth muscle cell
MYH9	myosin heavy chain 9
NMMHC-IIA	non-muscle myosin heavy chain II-A
RACE	rapid amplification of cDNA ends
RIP	RNA immunoprecipitation
scRNA-seq	single-cell RNA-seq
TPRG1-AS1	tumor protein p63 regulated 1, antisense 1
VSMC	vascular smooth muscle cell

Highlights

- TPRG1-AS1 (tumor protein p63 regulated 1, antisense 1) significantly increased in atherosclerotic plaques, was identified as bona fide a lncRNA, and characterized with the full length of transcript and the subcellular location in human aortic smooth muscle cells.
- Functionally, TPRG1-AS1 could regulate human aortic smooth muscle cells migration rather than proliferation.
- Mechanistically, TPRG1-AS1 directly interacted with MYH9 (myosin heavy chain 9) protein in human aortic smooth muscle cells, promoted MYH9 protein degradation and hindered F-actin stress fiber formation.
- Vascular smooth muscle cell–specific transgenic overexpression of TPRG1-AS1 significantly reduced neointima formation and attenuated atherosclerosis in apolipoprotein E knockout (*Apoe*$^{-/-}$) mice.

Atherosclerotic cardiovascular diseases, such as coronary artery disease (CAD),[1,2] cerebral infarction,[2] and peripheral vascular diseases,[3] are main causes of morbidity and mortality worldwide.[4] The most distinctive feature of atherosclerotic cardiovascular diseases is the formation of atherosclerotic plaque. The majority of cells in atherosclerotic plaque are derived from migrated vascular smooth muscle cells in media.[5] The thickening of vascular intima caused by aberrant proliferation and migration from the media to the intima of vascular smooth muscle cells (VSMCs) triggers vascular remodeling,[6] which is the critical step in the pathogenesis of atherosclerosis and restenosis after coronary angioplasty.[7-10]

Long noncoding RNAs (lncRNAs), widely expressed in mammals, are a class of RNA molecules with a length longer than 200 nucleotides (nt) and rarely encode proteins.[11–13] LncRNAs play an extensive role in various biological activities including chromatin remodeling, alternative splicing, genomic imprinting, cell cycle regulation, and so on,[14–16] by regulating gene expression at the transcriptional, posttranscriptional, and epigenetic levels. Several lncRNAs were reported to play crucial roles in regulating VSMC phenotype switching via interacting with proteins. For example, lncRNA AK098656 induced VSMC phenotype switching by promoting MYH11/FN1 protein degradation.[17] Antisense noncoding RNA in the INK4 locus (ANRIL) acted as a modular scaffold of WDR5 and HDAC3 complexes and promoted human aortic smooth muscle cell (HASMC) phenotype transition.[18] Cardiac mesoderm enhancer-associated noncoding RNA (CARMN) promoted a contractile phenotype of HCASMCs by directly binding to MYOCD.[19] However, the regulatory roles and underlying mechanisms of the overwhelming majority of lncRNAs in HASMCs phenotype switching and vascular remodeling need to be fully elucidated.

LncRNA TPRG1-AS1 (tumor protein p63 regulated 1, antisense 1) was a novel diagnostic biomarker for CAD based on transcriptome-wide lncRNA expression profile (GSE113079) in our previous study, and loss of TPRG1-AS1 regulated the expression of inflammation-related genes and its nearby genes in THP-1-derived macrophages.[20] However, the critical roles and underlying molecular mechanisms of TPRG1-AS1 in HASMCs phenotype switching and atherosclerosis remains unclear. The present study identified TPRG1-AS1 as a previously unrecognized inhibitor of HASMCs migration, neointima formation, and atherosclerosis through interacting with MYH9 (myosin heavy chain 9) protein.

MATERIALS AND METHODS

Data Access

The data that support the findings of this study are available from the corresponding author upon reasonable request.

Animals

The ROSA26 TPRG1-AS1 transgenic mice were generated by CRISPR/Cas9-based knock-in approach (Figure S1) by Beijing Biocytogen Co, Ltd. Briefly, sgRNAs were designed by CRISPR design tool (http://crispr.mit.edu). The gene targeting vector containing 5' homologous arm, target fragment (LSL-TPRG1-AS1), DSBs generated by Cas9/sgRNA were repaired by using 3' homologous arm as a template. The synthesized exogenous fragment was ligated into ROSA-based vector to form targeting vector. To add T7 promoter sequence to the Cas9 or sgRNA template, the PCR amplification in vitro was performed. Then, for fertilized C57BL/6N eggs at one-cell stage, the Cas9 mRNA, targeting vector, and sgRNAs were co-injected into its cytoplasm, which were transferred into oviducts of pseudopregnant Kunming female mice. Finally, F_0 mice with expected genotype were obtained. In order to establish germline-transmitted F_1 heterozygous mice, they were mated

with C57BL/6N mice. The genotype of F_0 and F_1 (TPRG1-AS1$^{loxp/loxp}$) heterozygous mice were further verified by tail genomic DNA PCR and sequencing, as well as southern blot. To produce VSMC-specific transgenic mice, TPRG1-AS1$^{loxp/loxp}$ mice were crossed with Tagln-Cre/+ mice and *Apoe*$^{-/-}$ mice to obtain VSMC-specific TPRG1-AS1 transgenic mice (TPRG1-AS1^{SMCKI}) with TPRG1-AS1$^{loxp/loxp}$ mice as control, and TPRG1-AS1^{SMCKI}*Apoe*$^{-/-}$ mice with TPRG1-AS1$^{loxp/loxp}$*Apoe*$^{-/-}$ mice as control, respectively. The genotype condition and primers are listed in Table S1. Sex is considered as a biological variable.[21] Estrogens have inhibitory effect on diet-induced atherosclerosis and neointimal formation after carotid artery injury of animal models as reported previously.[22,23] Therefore, to accelerate lesion formation, only male animals were used in the present study. Male TPRG1-AS1^{SMCKI} mice and their age-matched male control littermates were used for carotid wire injury model and primary cell isolation. Male TPRG1-AS1^{SMCKI}*Apoe*$^{-/-}$ mice and their age-matched male control littermates were used for atherosclerotic model. All animals were housed at controlled temperature (22±2 °C) and humidity (55±5%) with a 12:12 hours light-dark cycle. All animal experiments were performed in accordance with relevant guidelines and regulations and were approved by the Animal Care and Use Committee at Fuwai hospital, China.

Animal Experimental Design

The design of atherosclerosis model was in compliance with the guidelines for experimental atherosclerosis studies described in the AHA Statement.[24] The sample size was calculated by Power Analysis and Sample Size (PASS) software (PASS 15.0.5) with a level of significance of 0.05 and a power of 0.9. TPRG1-AS1^{WT} and TPRG1-AS1^{SMCKI} mice were housed together randomly in multiple cages to reduce cage bias. All animals were fed with the standard laboratory diet (Beijing HFK Bioscience Co, Ltd, 1025). The diets of 8-week-old TPRG1-AS1^{SMCKI}*Apoe*$^{-/-}$ and control mice (20-30g) were switched to high-fat diet (HFD, Beijing HFK Bioscience Co., Ltd, H10141) for 20 weeks (study endpoint). The information of animal diet was described in Table S2. Body weight was monitored weekly throughout the HFD feeding period. The mice plasma and whole aortas were collected after 20 weeks. Total cholesterol (TC) and triglyceride (TG) levels were measured with assay kits (Zhongshengbeikong Biotech Co, Ltd, China) according to the manufacturer's protocol. All quantitative analysis of images were performed in a blinded fashion to genotype. For animal experiments, mice were anesthetized with mixed anesthetic (9 mg sodium pentobarbital, 0.4 ml propylene glycol, 0.1 ml 95% absolute ethanol, 0.5 ml normal saline per milliliter) by intraperitoneal injection, and Sprague-Dawley rats were anesthetized with pentobarbital sodium (30 mg/kg bodyweight, IP) as previously described.[25] The adequacy of anesthesia and euthanasia was confirmed by the absence of reflex response to foot squeeze. Carbon dioxide (CO_2) euthanasia box and an intraperitoneal injection of sodium pentobarbital (40 mg/kg) were used for euthanasia.

En face Oil Red O Staining

As previously described,[24] the mice aortas harvested after high-fat diet feeding were processed for en face Oil red O staining. Briefly, fat and adventitial tissues of the aorta were carefully removed under a dissecting microscope and the aorta was cut longitudinally to expose the intimal surface followed by staining with freshly made Oil red O (ORO). Excess oil red O solution was removed by methanol. Plaque area analysis was carried out using Image Pro Plus software version 6.0 (RRID:SCR_016879, Media Cybernetics, Inc).

Atherosclerotic Lesion Quantification of Aortic Root

The hearts of diet-induced mice were embedded in paraffin. As previously described,[24] the aortic root from the origin of the aortic valve leaflets to the ascending aorta was evenly sliced into 5-μm several serial sections. For atherosclerotic lesion quantification, 3 serial sections from the first appearance of all 3 valve leaflets were collected at 80-μm intervals. The plaque area was calculated as the difference between the total aortic root area and aortic root luminal area, which was reported as the average of 3 sections. The plaque area and positive area analysis was carried out using ImageJ software (NIH, RRID:SCR_003070).

Tissue Samples

The carotid atherosclerotic plaques of patients undergoing carotid endarterectomy and the internal mammary artery specimens were obtained from Fuwai Hospital (Beijing, China). The ethical approval of this study protocol was obtained from the Ethics Committee of Fuwai Hospital. In accordance with the Declaration of Helsinki, the written informed consent was obtained from all participants or their families. The clinical information of patients was described in Table S3.

Bioinformatics Analysis of Public Microarray Datasets and Bulk RNA-seq Datasets

To compare the expression of TPRG1-AS1 in human normal arterial intimae and advanced atherosclerotic plaques, microarray data of 3 advanced atherosclerosis samples and 3 normal intima tissues (GSE97210) were analyzed using NCBI online GEO2R tool and annotated with the annotation file of Agilent-045997 Arraystar human lncRNA microarray V3 (GPL16956). To explore the expression pattern of TPRG1-AS1 in stable and unstable regions of human atherosclerotic plaques, Fragments Per Kilobase of exon per Million fragments mapped (FPKM) values of RNA sequencing data (GSE120521) were downloaded from the Gene Expression Omnibus (GEO) (RRID:SCR_005012). Normalized expression value of TPRG1-AS1 for each sample in each group was used for analysis and visualization.

Single-Cell RNA-Seq Analysis

To explore the expression of MYH9 gene in different types of vascular cells, single-cell RNA-seq (scRNA-seq) datasets of human coronary arteries (GSE131778) and aortic root and ascending aorta of SMC lineage tracing *Apoe*$^{-/-}$ mice at baseline, after 8 weeks or after 16 weeks of HFD feeding (GSE131776) were downloaded from GEO database. The R package Seurat was applied for the quality control, dimensionality reduction, and clustering of cell subpopulations. We performed principal component analysis and reduced the data to the top 30 principal component analysis components after

scaling the data. We visualized the clusters on a 2D map produced with t-SNE and identified cell types and subtypes by nonlinear dimensional reduction. Cells were clustered using graph-based clustering of the principal component analysis reduced data with the Louvain Method after computing a shared nearest neighbor graph. For each cluster, the Wilcoxon Rank-Sum Test was used to find significant deferentially expressed genes comparing the remaining clusters. SingleR and known marker genes were used to identify cell type. The t-distributed stochastic neighbor embedding (t-SNE) was used to visualize the normalized data of MYH9 gene in different cell clusters on a 2D map.

Cell Culture, Transfection, and Infection

Cells were cultured at 37 °C in an incubator with 5% CO_2. All cell lines were tested negative for mycoplasma contamination. HASMCs were used from passages 3 to 6 in the following experiments. Cells were seeded at a density of 1.0×10^5 cells per well in a 12-well plate 24 hours prior to the transfection, and transfected with 50 nM of the indicated siRNAs (Table S3) using Lipofectamine™ RNAiMax (Invitrogen) according to the manufacturer's instructions. For adenovirus mediated overexpression, Ad-TPRG1-AS1 or Ad-MYH9 (Vigenebio, Shandong, China) was added into the culture medium for 48 hours. A recombinant adenovirus encoding enhanced GFP (Ad-GFP) was used as a negative control.

Quantification of Copy Number

The solution of TPRG1-AS1 recombinant plasmids was gradient-diluted. Then, the Ct values of TPRG1-AS1 of serial dilutions of plasmids and RNA isolated from a defined amount of HASMCs were determined by qPCR assay. The Ct values of TPRG1-AS1 of serial dilutions of plasmids were used to construct the standard curve equation (logarithmic value with the amplification starting copy number taken 10 as the ordinate [y] and corresponding cycle number as the abscissa [x]). The copy number of TPRG1-AS1 in HASMCs per cell is calculated according to number of cells and Ct values. Each biological replicate included 3 technical replicates.

RACE Assay

The full-length transcript of TPRG1-AS1 was confirmed using rapid amplification of cDNA ends (RACE) assay, which were performed using the SMARTer RACE 5′/3′ Kit (Clontech Laboratories, Mountain View, CA) according to the manufacturer's instructions. For the nested PCR, we designed and synthesized at least 2 sets of primers. The PCR products were separated on a 1.0% agarose gel. The results of electrophoresis were confirmed, and the amplified bands were sequenced by cloning to the pEASY-Blunt Simple and then translate to Trans T1 bacteria. Single colonies were selected for sequencing and the sequencing results were compared and analyzed. The cycling parameters were: RACE 25×(94 °C 30 seconds, 68 °C 30 seconds, 72°C 3 minutes). The sequences of the oligonucleotide primers and probes used for the reverse transcription RACE PCR were described in Table S7.

Northern Blot

Briefly, total RNA was extracted from HASMCs using Trizol reagent (Invitrogen life technologies, Carlsbad, CA). For 7.5 M urea-12% formaldehyde (PAA) denaturing gel electrophoresis, we used 20 μg of total RNA, which was transferred to a Hybond N+ nylon membrane (Amersham, Freiburg, Germany). The membrane was crosslinked by UV irradiation for 2 min. The antisense DNA probe of TPRG1-AS1 was used for hybridization. The membrane was washed 2× with 2×SSC+0.1% SDS solutions (Invitrogen life technologies, Carlbad, CA) at 42 °C for 20 minutes. And then the membrane was exposed to Kodak XAR-5 films (Sigma-Aldrich Chemical). As a positive control, all the membranes were hybridized with human U6 probe. All the probe sequences were described in Table S8.

RNA Immunoprecipitation Assay

According to the manufacturer's instructions, RNA immunoprecipitation (RIP) assay was performed using EZ-Magna RIP RNA-Binding Protein Immunoprecipitation Kit (Millipore-17-701). Then, 2.0×10^6 HASMCs were lysed in 100 μL RIP lysis buffer, and the whole cell extract (90 μL) was incubated with human anti-MYH9 antibody (ab238131; Abcam, Cambridge, MA) or negative control rabbit IgG (ab172730; Abcam, Cambridge, MA) in RIP buffer containing protein complexes bound by A/G magnetic beads. The TPRG1-AS1 levels in the precipitates were determined by qPCR. Two independent TPRG1-AS1 primers used for RIP assay were described in Table S9.

RNA Pull-Down, Silver Staining, and Mass Spectrometry Analysis

For biotinylated RNA generation, PCR products were used for in vitro transcription with T7 RNA polymerase (Roche, Catalog No. 10881767001). The RNA was biotinylated at its 3′ end, using the Biotin Labeling Mix (Roche, Catalog No. 11685597910). Biotinylated RNA probes were incubated with streptavidin magnetic beads (Invitrogen, Catalog No. 15942-050) according to the manufacturer's instructions. Total cellular proteins were extracted by RIPA lysis buffer containing complete protease inhibitor (Roche, Germany). A total of 1 mg total cellular proteins was added to the RNA-bound streptavidin magnetic beads, and the complex was incubated at room temperature for 1 hour. The complex was then centrifugated at a speed of 1000 rpm for 10 minutes and was washed 3 times with wash buffer. The RNA-bound proteins were eluted in 50 μL 5×SDS sample buffer, denaturized at 95 °C for 10 minutes, and resolved by SDS-PAGE on 8% acrylamide gel (Bio-Rad, Hercules, CA). RNA-bound proteins were visualized by silver staining (Beyotime, China, Cat. P0017S), and protein bands of interest were excised and sequenced by mass spectrometry (MS) at Shanghai LuMing Biological Technology Co. Ltd (Shanghai, China).

Chromatin Isolation by RNA Purification Assay

Chromatin isolation by RNA purification experiment was used to validate the target protein that is directly binding to TPRG1-AS1. Protein-RNA interactions were measured according to the manufacturer's instructions. Briefly, 20-mer antisense DNA probes targeting TPRG1-AS1 RNA, as well

as the negative control lacZ RNA, were designed such that 1 probe covered every 100 bp of RNA, with a target GC% of 45. All probes were biotinylated at the 3' end. First, cultured cells (>2.0×10^6 cells) were UV cross-linked by 240 to 960 mJ, and 1 mL pre-cooled PBS containing 10 µL Halt Cocktail was added, the cells were scraped off. 1 mL lysis buffer suspension cells containing protease inhibitors were added to the UV cross-linked cells. If viscous substances were produced, the genome could be disrupted by ultrasound treatment. TPRG1-AS1 and its interacting proteins were precipitated using Streptavidin Magnetic Beads (Invitrogen, CA). RNA was eluted with RNA pK buffer and Proteinase K and then isolated using Trizol reagent. Protein was eluted with a cocktail of RNase A (Sigma-Aldrich) and RNase H (Epicenter), and DNase I (Invitrogen). TPRG1-AS1 isolation was validated by quantitative real-time polymerase chain reaction (qRT-PCR) analysis, and proteins were identified by Western blot. Primers and probes used for chromatin isolation by RNA purification assay were described in Tables S9 and S10, respectively.

Secondary Structure Prediction for LncRNA TPRG1-AS1

The secondary structure of the full-length sequence of LncRNA TPRG1-AS1 was predicted on RNAfold WebServer (http://rna.tbi.univie.ac.at/cgi-bin/RNAWebSuite/RNAfold.cgi) based on the minimum free energy (MFE).

RNA Fluorescence In Situ Hybridization

RNA fluorescence in situ hybridization was used to determine the localization of TPRG1-AS1 in HASMCs. The cell slides were placed on the bottom of the 24-well plate, and then a certain number of cells (6×10^4) were seeded on the cell slide. After 24 hours of culture, the cell fusion reached 60% to 70%, then the cell slides were fixed with 4% of formaldehyde solution for 20 minutes. In brief, after fixation, slides were incubated with cold permeable solutions for 5 minutes at 4 °C and prehybridized for 30 minutes at 37 °C. Hybridization with DIG-labeled TPRG1-AS1 probes or DIG-labeled U6 probes (Ribobio, China) was performed overnight at 37 °C, respectively. Next, the cell slides were washed with PBS and incubated with DAPI staining solutions (Invitrogen, Carlsbad, CA) for 10 minutes at room temperature. Glass slides were mounted on slides using fluorescence mounting medium (Antifade) (Beyotime, Beijing, China). Fluorescence was detected with laser scanning confocal microscope (Olympus, Tokyo, Japan). U6 was used as the internal reference (all the experiments performed according to the manufacturer's instructions). The reagents used have been listed in Major Resources Table.

RNA Isolation and Quantitative Real-Time Polymerase Chain Reaction

Total RNA from HASMCs was isolated with TRIzol reagent (Invitrogen, Carlsbad) according to the manufacturer's protocol. RNA quantity was assessed using NanoDrop 2000 (NanoDrop Products, Wilmington, DE). One micrograms of total RNA was reverse transcribed using a Transcriptor First Strand cDNA Synthesis Kit (Roche, Germany) according to manufacturer's instructions. qRT-PCR was done with an ABI PRISM 7900 system (Applied Biosystems, Foster City) according to standard methods. Primers used for qRT-PCR were described in Table S5. The relative mRNA expression levels were calculated using the $2^{-\Delta\Delta ct}$ method normalized to the housekeeping gene glyceraldehyde-3-phosphate dehydrogenase (GAPDH). Each biological replicate included 3 technical replicates.

Western Blotting

Cells were lysed with RIPA buffer containing complete protease inhibitor (Roche, Germany) for 30 minutes on ice, lysate was centrifuged at 12 000 rpm for 5 minutes at 4 °C and the supernatant was retained. An equal amount of protein samples was loaded into a 10% SDS-polyacrylamide gels or a 4% to 12% Bris-Tris gel (GenScript) and then electroblotted to nitrocellulose membrane. Band density was quantified using Quantity One 1-D Analysis Software (Bio-Rad Laboratories, CA, RRID:SCR_014280). The antibodies used have been listed in Major Resources Table. Please see the Major Resources Table in the Supplemental Material.

Cell Proliferation Assay

For the proliferation assays in vitro, HASMCs (1×10^5 cells/well) were seeded in 96 well-plates and incubated for 24 hours. After experiment treatment at 0, 24, 48, 72 hours, 10 µL of WST-8solution(2-[2-methoxy-4nitrophenyl]-3-[4-nitrophenyl]-5-[2,4-disulfophenyl]-2H-tetrazolium, monosodium salt) was added into each well. Three biological replicates were used for each experimental group (Each biological replicate included 5 technical replicates). Plate was incubated for 2 hours in an incubator with 5% CO_2 at 37 °C, and then the absorbance value was measured at 450 nm using a microplate reader.

Cell Migration Assay

Migration assays were performed with transwell plates with 8-µm pore size (3422; Costar, Cambridge, MA). The cell density was adjusted to 3.0×10^5/mL, and 100 µL cell suspension was added to the top chamber of a 24-well transwell plate. The serum-free SMCM medium was added in the upper chamber, and the medium in the lower chamber was supplemented with 10% FBS. After incubation for 24 hours at 37 °C, the noninvasive cells were removed with a cotton swab. The cells passing through the filter into the bottom wells were fixed in 4% formaldehyde solution for 30 minutes and stained with Crystal Violet Staining Solution (Beyotime Biotechnology, China) for 15 minutes, and those migrated cells were counted using an Olympus microscope equipped with a camera (Leica, Germany), the migrated cells were counted using ImageJ software (RRID:SCR_003070). Six biological replicates were used for each experimental group.

F-Actin Staining

The HASMCs were cultured on cell slides in 12-well plates, at the bottom of which cell climbing plates were placed in advance. After treatment, cells were washed twice with PBS and then fixed with 4% paraformaldehyde solution for 30 minutes at room temperature. Cell slides were rinsed with PBS, permeabilized with PBS containing 0.1% Trixon X-100 for 5 minutes. Cells were then blocked with 1% BSA for 20 minutes

at room temperature. Phalloidin (1:1000, F-actin Staining Kit-Red Fluorescence-Cytopainter, ab112127) was then added to the cell slides at dilutions of 1:1000 and incubated at room temperature for 90 minutes. After incubation, rinsed twice with PBS, and proLongTM Gold anti-fade mountant with DAPI (Thermo Fisher Scientific, P36935) was added to cell slides for 10 min, and then acquired the images with a confocal microscope. Six biological replicates were used for each experimental group. The reagents used have been listed in Major Resources Table.

Isolation and Culture of Primary Mouse Aortic Smooth Muscle Cells

Male mice (TPRG1-AS1$^{fl/fl}$ and TPRG1-AS1$^{fl/fl}$Tagln$^{cre/+}$ mice,20-25g, 6–8 weeks old, n=8) were anesthetized with mixed anesthetic (9 mg sodium pentobarbital, 0.4 ml propylene glycol, 0.1 ml 95% absolute ethanol, 0.5 ml normal saline per milliliter) by intraperitoneal injection. The thoracic and abdominal cavities were opened, the heart was exposed, and the aorta was flushed with PBS buffer; The aorta was isolated intact, the adventitia of the vessel was dissected off microscopically, and the intima was gently scraped off with sterile forceps; The vessels were minced (1 mm×1 mm×1 mm), digested by 2 mg/ml collagen II with magnetic stirring at 37 °C for about 1 hour, centrifuged at 1500 rpm for 5 minutes, discarded the supernatant, resuspended with high glucose DMEM medium containing 20% FBS, and statically cultured for 2 to 3 days. Mouse aortic smooth muscle cells (MASMCs) were used from passages 3 to 6 in the following experiments.

Balloon Injury Model

In brief, male Sprague-Dawley rats (350–400 g) were anesthetized according to the method described before, then the left carotid artery was exposed. The balloon dilation was performed to the left carotid artery of rats, and the sham littermate underwent the same procedures without the incision and injury. A 2.0 mm diameter balloon catheter (Medtronic, Minneapolis, MN) was inserted into the left common carotid artery via the external carotid. The balloon was inflated and withdrawn in the left common carotid artery for 3 times. After balloon injury, solutions (100 µL) of Ad- TPRG1-AS1 (1.5×10^8 PFU/mL) or Ad-GFP (1.5×10^8 PFU/mL) were infused into the ligated segment of the left common carotid artery for 30 minutes. Rats were anesthetized with intraperitoneal injection of pentobarbital sodium (40 mg/kg bodyweight) 14 days after the balloon injury, and the artery was collected, fixed in 4% paraformaldehyde for > 24 hours and embedded in paraffin.

Wire Injury of Carotid Artery

Briefly, TPRG1-AS1^{SMCKI} mice and control mice (10 weeks old) were anesthetized with mixed anesthetic (9 mg sodium pentobarbital, 0.4 ml propylene glycol, 0.1 ml 95% absolute ethanol, 0.5 ml normal saline per milliliter), and the left common carotid artery including bifurcation was exposed, dissected, and injured by passing a curved flexible wire (0.38-mm diameter, Reference Part Number: C-SF-15-20, Cook Medical European Shared Services, Ireland) five times toward and forth with rotation. The sham littermate (TPRG1-AS1^{SMCKI} and control) mice underwent the same procedures without the incision and injury. Carotid arteries were harvested 2 weeks after the injury. Carotid arteries were fixed in 4% paraformaldehyde for > 24 hours and embedded in paraffin.

Histochemistry and Immunofluorescence Staining

Paraffin embedded tissues were sectioned with a thickness of 5 µm for hematoxylin and eosin (HE) staining and immunofluorescence. HE staining was performed following standard procedures by automatic HE staining apparatus. The extent of neointimal formation and intima-to-media (I/M) area ratio was quantified using ImageJ software (RRID:SCR_003070). For immunofluorescence staining, the paraffin sections were blocked for 1 hour in the blocking buffer with goat serum and then were incubated with MYH9 antibody (ab75590) overnight at 4 °C after deparaffinization and antigen repair. After being rewarmed at 37 °C for 1 hour, the slices were washed with PBS and incubated with fluorescence-labeled secondary antibody (Alexa Fluor 488 goat anti-rabbit IgG (H+L), Thermo Fisher Scientific Cat# A-11008, RRID: AB_143165) at 37 °C for 1 hour. Cell nuclei were stained with DAPI, and images were captured using a confocal laser scanning microscope. The antibodies used have been listed in Major Resources Table. Please see the Major Resources Table in the Supplemental Material. The quantitative analysis of immunofluorescence images was performed using Image Pro Plus software version 6.0 (RRID:SCR_016879).

Statistical Analysis

All statistical analyses were performed using the GraphPad Prism 8.0 software (RRID:SCR_002798), SPSS 20.0 (RRID:SCR_002865) and R software (R version 4.1.3). Continuous variables were tested for normal distribution using the Shapiro-Wilk normality test. Levene and Brown-Forsythe tests were used to test the homogeneity of variances. Student *t* test (unpaired) or paired *t* test were used for 2-group analysis with equal variance, and Welch *t* test was used for 2-group analysis with unequal variance. One-way ANOVA with Tukey multiple comparison test was used for multiple group analysis. Two-way ANOVA test was used for analysis of 2 independent variables. Non-normally distributed data were compared using non-parametric tests. Mann-Whitney test was used for unpaired 2-group analysis. Wilcoxon signed-rank test was used for paired 2-group analysis. Kruskal-Wallis test with Dunn's multiple comparisons test was performed for multiple-group analysis. The data tested by parametric tests were shown as the mean and SEM, and data tested by nonparametric tests were represented as median with 95% confidence limits. Fisher exact probability method was used to compare categorical variables between 2 groups. N values in the figure legend represent the number of independent biological replicates unless otherwise indicated specifically. $P<0.05$ was thought to be statistically significant.

RESULTS

Characterization of TPRG1-AS1 as a lncRNA

Information from Ensembl shows that TPRG1-AS1 (RefSeq: NR_046873) localized on human Chromosome 3:

188,941,715-188,947,639 (the minus strand) and had a transcript of 697 nt and consisted of 2 exons, with low conservation among 100 vertebrates (Figure S2A). To provide clues for the role of TPRG1-AS1 in the pathogenesis of atherosclerosis, we searched for disease-relevant tissues or cell types that express TPRG1-AS1 in the expression data from the Genotype-Tissue Expression project[26] and GEO dataset. The data from Genotype-Tissue Expression demonstrated that human arterial tissue, including aorta and coronary arteries expressed TPRG1-AS1 (Figure 1A). The TPRG1-AS1 expression was detected by qRT-PCR in atherosclerotic plaques collected from patients undergoing carotid endarterectomy and internal mammary artery specimens obtained during coronary artery bypass surgery, and the TPRG1-AS1 expression was significantly higher in carotid atherosclerotic plaques than internal mammary artery (Figure 1B). Reanalyzing lncRNA/mRNA expression profile for human normal arterial intimae and advanced unstable atherosclerotic plaques (GSE97210)[27] showed that TPRG1-AS1 expression was markedly increased in atherosclerotic plaques (Figure 1C). Then, reanalyzing RNA sequencing data of stable and unstable section of human atherosclerotic plaques (GSE120521)[28] demonstrated that the expression level of TPRG1-AS1 was significantly increased in unstable region (Figure 1D). To figure out the expression levels of TPRG1-AS1 in different cell types of human atherosclerotic coronary artery, we reanalyzed the scRNA-seq dataset (GSE131778),[29] and we found that the expression level of TPRG1-AS1 was not significantly different in endothelial cell, vascular smooth muscle cells, monocytes, macrophages, fibroblasts and foam cells of human atherosclerotic coronary artery (Figure S3A), though a relatively higher expression level of TPRG1-AS1 in HASMCs than in HUVECs confirmed by Northern blot (Figure S3B). In comparison with protein coding genes, the abundance of lncRNA is significantly lower. By absolute copy number analysis,[30] the copy number of TPRG1-AS1 is calculated as ~9 copies per cell, which is similar to the abundance of a number of lncRNAs[31] (Figure S4). Owing to the critical regulatory role of VSMC phenotype switching in the pathogenesis of atherosclerosis, we wondered whether TPRG1-AS1 might regulate VSMC phenotype switching. The expression pattern of TPRG1-AS1 was detected in HASMCs treated by PDGF-BB, a growth factor known to promote VSMC phenotype switching in the pathogenesis of atherosclerosis.[32] Exposure to PDGF-BB downregulated TPRG1-AS1 by 30% in HASMCs (Figure 1E), suggesting the possible involvement of TPRG1-AS1 in HASMCs phenotype switching.

Using known sequence of TPRG1-AS1, we designed primers and performed 5' and 3' RACE to obtain the full-length transcript of TPRG1-AS1(Figure 1F). The 5'- and 3'- RACE (Figure S5) and subsequent Sanger sequencing showed that the full-length transcript of TPRG1-AS1 was 1279 nt in length, with a poly(A) tail (Table S6), consistent with the size of the transcript of TPRG1-AS1 determined by Northern blot in HASMCs (Figure S3B). Because the function of lncRNA is dependent on its subcellular localization, RNA fluorescent in situ hybridization was performed to determine the subcellular localization of TPRG1-AS1 in HASMCs. The result demonstrated that endogenous TPRG1-AS1 was localized in both the cytoplasm and nuclear of HASMCs, but mainly in cytoplasmic and peri-nuclear regions (Figure 1G). TPRG1-AS1 showed little coding potency by the PhyloCSF analysis (Figure S2B) and did not have a representative protein-coding open reading frame longer than 243 nt among the fourteen open reading frames according to open reading frame Finder[24] (Figure S2C and S2D). Finally, in vitro transcription-translation assay demonstrated that TPRG1-AS1 did not code any proteins (Figure 1H) and thus confirmed that TPRG1-AS1 was *bona fide* a lncRNA.

TPRG1-AS1 Inhibits HASMCs Migration

Loss- and gain-of function strategies were adopted to explore the function of TPRG1-AS1 in HASMCs phenotype switching. TPRG1-AS1 was efficiently overexpressed in HASMCs infected with Ad-TPRG1-AS1 (Figure 2A), and endogenous TPRG1-AS1 was successfully knocked down to about 6% in HASMCs transfected with si-TPRG1-AS1(Figure 2B). The expression of TPRG1, the parent gene of TPRG1-AS1 was not affected by the knockdown of TPRG1-AS1 in HASMCs (Figure S6). The overexpression or knockdown of TPRG1-AS1 did not significantly affect the expression of contractive markers (Figure S7A and S7B) and HASMCs proliferation detected by CCK-8 assay (Figure S7C and S7D). Transwell migration assay was performed to investigate the effect of TPRG1-AS1 on HASMCs migration. The overexpression of TPRG1-AS1 significantly and drastically inhibited HASMCs migration (Figure 2C and 2D), while the knockdown of TPRG1-AS1 had an opposite effect (Figure 2E and 2F). Furthermore, the overexpression of TPRG1-AS1 also significantly inhibited HASMCs migration induced by PDGF-BB (Figure 2G and 2H).

TPRG1-AS1 Directly Interacts With MYH9 Protein in HASMCs

Growing evidence has demonstrated that lncRNAs could participate in molecular regulation pathways through physically interacting with proteins.[17,19] The multiple-branched structure predicted by RNAfold server (http://rna.tbi.univie.ac.at/cgi-bin/RNAWebSuite/RNAfold.cgi) suggested the binding potential of TPRG1-AS1 with protein (Figure S8). To identify intracellular binding proteins via which TPRG1-AS1 inhibited HASMCs migration, we performed RNA pull-down assay with protein lysate

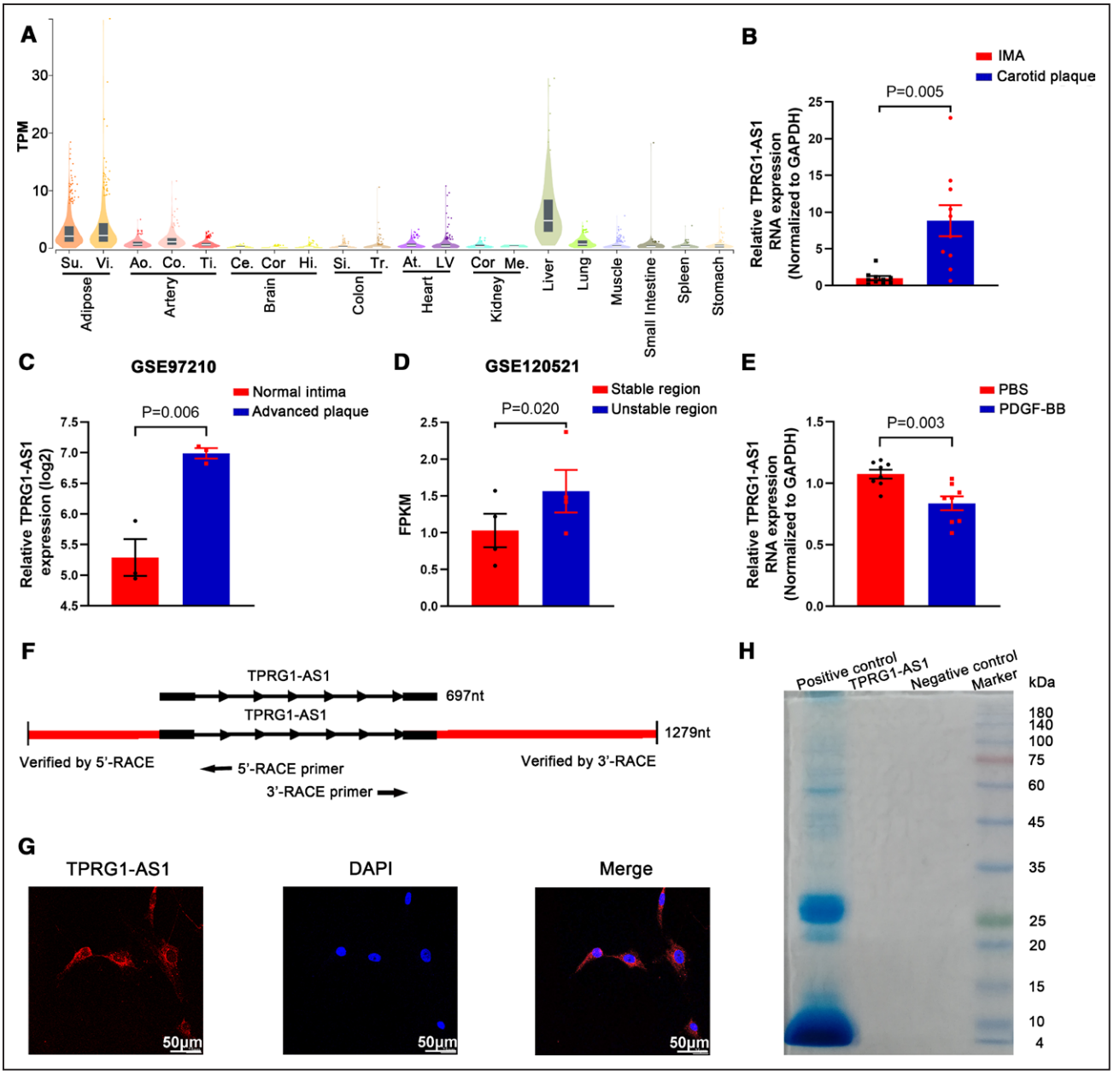

Figure 1. Characterization of TPRG1-AS1 (tumor protein p63 regulated 1, antisense 1) as a lncRNA.
A, TPRG1-AS1 expression across different human tissues in the GTEx database. **B**, The expression of TPRG1-AS1 in human carotid atherosclerotic plaques and internal mammary arteries (IMA; n=10 per group). **C**, Reanalysis of TPRG1-AS1 expression in microarray datasets (GSE97210). **D**, Reanalysis of TPRG1-AS1 expression in RNA-seq datasets (GSE120521). FPKM: Fragments Per Kilobase per Million. **E**, The downregulation of TPRG1-AS1 expression in human aortic smooth muscle cells (HASMCs) induced by PDGF-BB (n=6 per group). **F**, The 5', 3'-terminal unknown sequences clone strategy of TPRG1-AS1 in HASMCs by rapid-amplification of cDNA ends (RACE). **G**, Representative pictures of FISH used to detect the subcellular localization of TPRG1-AS1 in HASMCs. TPRG1-AS1 were stained with specific probe of TPRG1-AS1 (red), nuclear were stained with DAPI (blue). Scale bars, 50 μm. **H**, Representative pictures of in vitro transcription-translation assay for TPRG1-AS1, positive control (T7 luciferase control DNA, 61kD), and negative control (no DNA). Data were expressed as mean±SEM. Results in **B** were evaluated by Welch test. Results in **C**–**E** were evaluated by Welch test. Ao indicates aorta; At, atrial appendage; Ce, cerebellum; Co, coronary; Cor, cortex; Hi, hippocampus; LV, left ventricle; Me, medulla; Si, sigmoid; Su, subcutaneous; Ti, tibial; TPM, Transcripts Per kilobase Million; Tr, transverse; and Vi, visceral.

from HASMCs followed by liquid chromatograph-mass spectrometer analysis. The full-length of TPRG1-AS1 was used as baits by generating both sense and antisense (negative control) RNA probes. Two differentially displayed protein bands (bands 1-2 numerically labeled on the gel, arrowed in Figure S9) were identified on the silver-stained polyacrylamide gel, and these 2 differential bands were excised and subjected to mass spectrometry. Mass spectrometry identified several potential TPRG1-AS1-interacted proteins, including MYH9 (Figure 3A). There might be a direct interaction between TPRG1-AS1 and MYH9 protein according to the

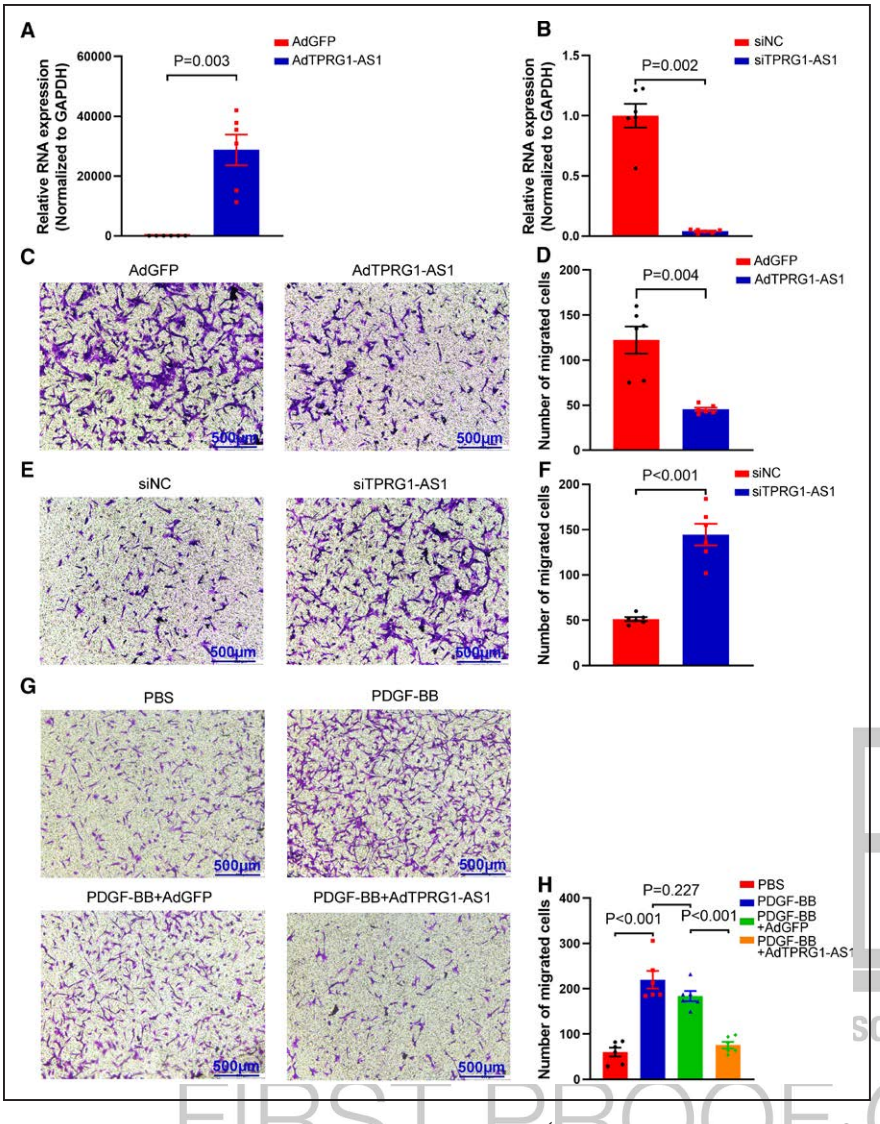

Figure 2. TPRG1-AS1 (tumor protein p63 regulated 1, antisense 1) inhibits human aortic smooth muscle cells (HASMCs) migration.
A, The overexpression of TPRG1-AS1 in HASMCs (n=6 per group). **B**, The knockdown of TPRG1-AS1 in HASMCs (n=6 per group). **C**, Representative pictures of the effect of the overexpression of TPRG1-AS1 on HASMCs migration. Scale bars, 500 μm. **D**, The statistical result in **C** (n=6 per group). **E**, Representative pictures of the effect of the knockdown of TPRG1-AS1 on HASMCs migration. Scale bars, 500μm. **F**, The statistical result in **E** (n=6 per group). **G**, Representative pictures of the effect of the overexpression of TPRG1-AS1 on HASMCs migration induced by PDGF-BB. Scale bars, 500 μm. **H**, The statistical result in **G** (n=6 per group). Data were expressed as mean±SEM. Results in **A**, **B,** and **D** were evaluated by Welch test. Results in **F** were evaluated by Student *t* test. Results in **H** are evaluated 1-way ANOVA followed by Tukey multiple comparison test.

RNA-protein interaction prediction tool RPIseq (http://pridb.gdcb.iastate.edu/RPISeq/; Figure 3B). The direct interaction between TPRG1-AS1 and MYH9 protein in HASMCs was verified by RIP assay, and GAPDH were used as negative controls. TPRG1-AS1 was significantly enriched by MYH9 protein antibody compared with IgG-controls (Figure 3C and 3D), demonstrating a direct interaction between TPRG1-AS1 and MYH9 protein in HASMCs. In addition to TPRG1-AS1, 2 other lncRNAs MAFG-AS1[33]and TP53TG1[34] with high abundance in HASMCs (Figure S10A), previously reported to bind to MYH9 protein in other type cells, also interacted with MYH9 protein in HASMCs (Figure S10B). To further validate the interaction of TPRG1-AS1 with MYH9 protein in HASMCs, we performed chromatin isolation by RNA purification assay, an optimized method for the identification of lncRNA-bound proteins. We designed 13 probes against TPRG1-AS1 RNA, and probes against lacZ RNA were used as negative control. The result of qPCR on the biotinylated probe-bound fraction confirmed that only biotinylated probes specific to TPRG1-AS1, enriched TPRG1-AS1 rather than non-specific transcript of GAPDH, and the lacZ control enriched neither TPRG1-AS1 nor GAPDH. Thus, these data validated the specificity of the probes used to retrieve TPRG1-AS1 in the chromatin isolation by RNA purification assay (Figure 3E). Subsequent Western blot showed that MYH9 protein could be retrieved by TPRG1-AS1 probes, but not LacZ control probes (Figure 3F), demonstrating that TPRG1-AS1 could bind to MYH9 protein in HASMCs. Taken together, the results confirmed the direct interaction of TPRG1-AS1 with MYH9 protein in HASMCs.

We sought to determine the function of the interaction between TPRG1-AS1 and MYH9 protein. Numerous studies have reported that some lncRNAs directly bind to protein and promote its degradation.[17,35] In the present study, a significant downregulation of MYH9 protein was detected in TPRG1-AS1-overexpressing HASMCs (Figure 3G and 3H), but no decrease was observed in MYH9 mRNA levels (Figure S11A). A significant upregulation of MYH9 protein upon TPRG1-AS1 knockdown was detected in HASMCs (Figure 3I and 3J) and no increase

A

1# band of mass spectrometry analysis of the proteins pulled down by TPRG1-AS1

Hits	Description	Score	Mass (kDa)	Matches	Sequences	emPAI
1	**Myosin-9(MYH9)**	1965	227646	126 (85)	50 (35)	0.77
2	Serum albumin	1491	71317	75 (58)	30 (28)	2.69
3	Unconventional myosin-Ic	1112	122461	82 (49)	35 (24)	0.93
4	Actin, cytoplasmic 1	667	42052	36 (27)	11 (9)	1.3
5	Drebrin	644	71842	36 (27)	9 (9)	0.64

2# band of mass spectrometry analysis of the proteins pulled down by TPRG1-AS1

Hits	Description	Score	Mass (kDa)	Matches	Sequences	emPAI
1	Serum albumin	1824	71317	81 (64)	33 (27)	2.37
2	Tubulin beta chain	1032	50095	45 (41)	12 (12)	1.6
3	**Myosin-9(MYH9)**	850	227646	49 (33)	24 (17)	0.27
4	Tubulin alpha-1C chain	767	50548	31 (27)	11 (10)	0.88
5	Lupus La protein	728	46979	32 (23)	12 (8)	0.84

B

RPIseq Prediction

Protein	RF classifier	SVW classifier
MYH9	**0.75**	**0.77**

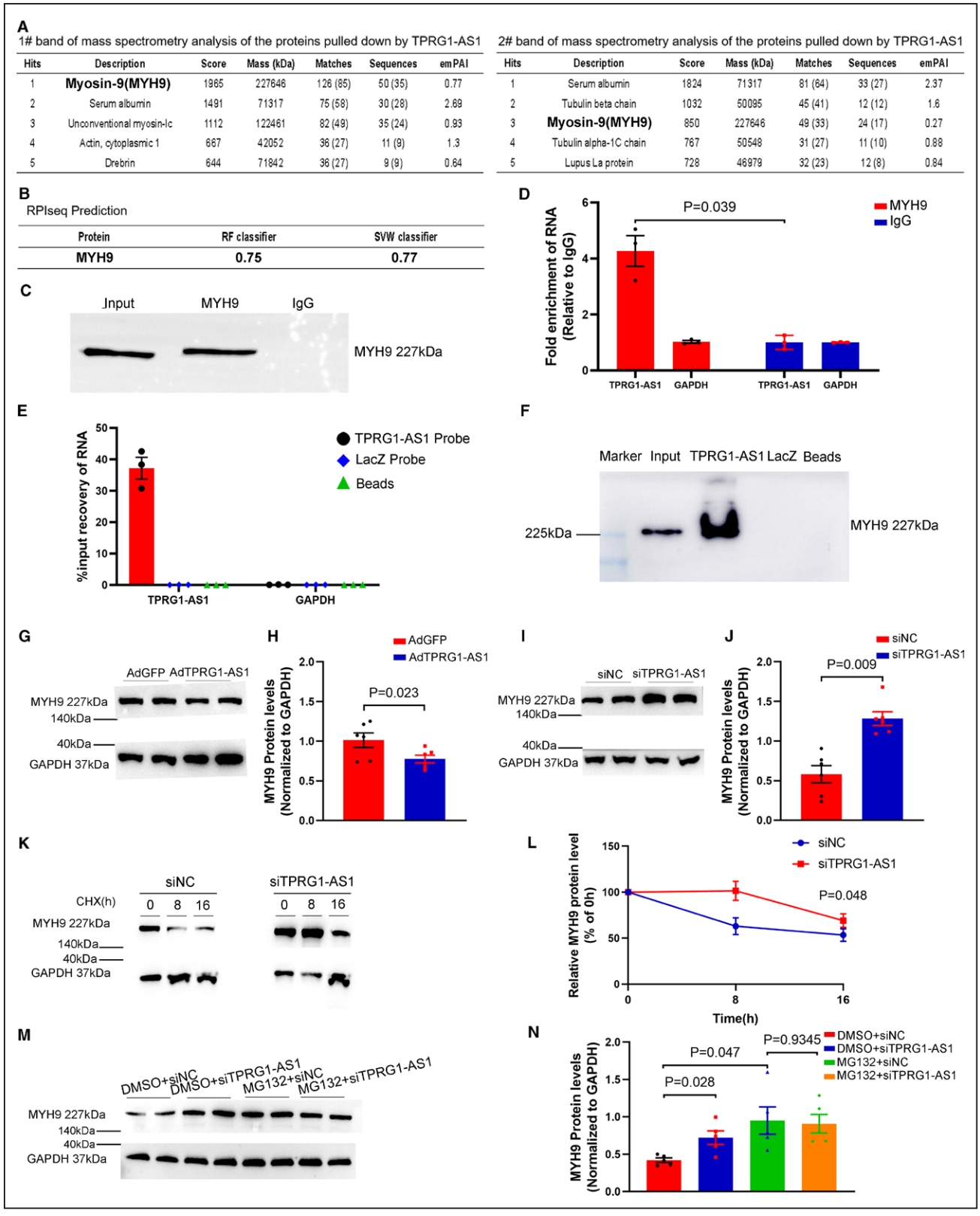

Figure 3. TPRG1-AS1 (tumor protein p63 regulated 1, antisense 1) directly interacts with MYH9 (myosin heavy chain 9) protein in human aortic smooth muscle cells (HASMCs).

A, The results of mass spectrometry analysis of 1# and 2# bands. **B**, The prediction of interaction between TPRG1-AS1 and MYH9 protein by RPIseq. **C**, Western blotting of proteins retrieved by MYH9-specific antibody and IgG in RIP assay of UV-crosslinked HASMCs extracts. **D**, qPCR detection of TPRG1-AS1 RNA retrieved by MYH9-specific antibody compared with those retrieved by IgG in RIP assay of UV-crosslinked HASMCs extracts (n=3 per group). GAPDH is used as negative control. **E**, qRT-PCR was used to detect (*Continued*)

in MYH9 mRNA levels was observed (Figure S11B). To determine the effects of the interaction of TPRG1-AS1 with MYH9 protein on the half-life of MYH9 protein, HASMCs transfected with siNC or siTPRG1-AS1 were treated with protein synthesis inhibitor[36] CHX (cycloheximide) for 0, 8, 16h, and the result demonstrated that the half-life of MYH9 protein was prolonged upon TPRG1-AS1 knockdown in HASMCs (Figure 3K and 3L). Previous study has reported that MYH9 protein could be degraded by proteasome pathway.[36,37] To figure out the underlying mechanism by which TPRG1-AS1 promoted the degradation of MYH9 protein, TPRG1-AS1 knockdown and control HASMCs were treated with the proteasome inhibitor MG132 or DMSO as a control. Exposure to MG132 significantly inhibited the degradation of MYH9 protein in HASMCs, demonstrating that MYH9 protein could also be degraded through proteasome pathway in HASMCs. In HASMCs treated with DMSO, the expression level of MYH9 protein was significantly increased after TPRG1-AS1 knockdown, however, there were no significant changes of MYH9 protein levels between TPRG1-AS1 knockdown and control cells after MG132 treatment (Figure 3M and 3N), indicating that the knockdown of endogenous TPRG1-AS1 protected MYH9 protein from proteasome degradation.

TPRG1-AS1 Inhibits HASMCs Migration via Interacting With MYH9 protein

MYH9 protein, also known as NMMHC-IIA (non-muscle myosin heavy chain II-A), is a cytoskeleton F-actin-binding protein, taking center stage in cell adhesion and migration.[38–42] However, its role in HASMCs migration and atherosclerosis is far from being completely characterized. According to the expression data from the Genotype-Tissue Expression project, MYH9 mRNA is substantially highly expressed in aorta and coronary arteries (Figure 4A). The expression of MYH9 protein was rapidly and significantly increased in neointima in both rat and baboon balloon injury models.[43,44] Reanalyzing the scRNA-seq dataset (GSE131778)[29] showed that MYH9 mRNA was relatively highly expressed in VSMCs among different cell types in human atherosclerotic coronary arteries (Figure 4B) and significantly increased in phenotypically modulated SMCs compared with normal SMCs (Figure 4C). Furthermore, MYH9 protein was largely colocalized with smooth muscle (α-SMA positive) cells in human atherosclerotic plaque by immunofluorescence staining (Figure S12). Similarly, the data from the scRNA-seq dataset (GSE131776)[29] of aortic root and ascending aorta in *Apoe*$^{-/-}$ mice at baseline, 8 and 16 weeks of high-fat diet (HFD) feeding also demonstrated that Myh9 mRNA expression was significantly upregulated in phenotypically modulated SMCs compared with normal SMCs (Figure 4D; Figure S13) and also continued to increase in phenotypically modulated SMCs from *Apoe*$^{-/-}$ mice at baseline, 8 and 16 weeks of HFD (Figure 4E). The expression pattern of MYH9 gene in human atherosclerosis sample and animal atherosclerosis model indicated the involvement of MYH9 gene in VSMC phenotype switching and the pathogenesis of atherosclerosis.

The efficiency of the overexpression and knockdown of MYH9 gene in HASMCs was verified by qRT-PCR and Western blot, respectively (Figure S14A through S14F). The knockdown of MYH9 gene in HASMCs significantly inhibited migration (Figure 4F and 4G), and the overexpression of MYH9 gene significantly promoted HASMCs migration (Figure 4H and 4I). Also, the knockdown of MYH9 gene did not affect the expression of contractive markers (Figure S15A) and HASMCs proliferation (Figure S15B). Since the interaction between TPRG1-AS1 and MYH9 protein could decrease MYH9 protein level, it was speculated that the interaction between TPRG1-AS1 and MYH9 protein might be involved in the inhibition of HASMCs migration by TPRG1-AS1. Functionally, the knockdown of MYH9 gene could significantly attenuate the increase in HASMCs migration induced by the knockdown of TPRG1-AS1 (Figure 4J and 4K), demonstrating that TPRG1-AS1 inhibited HASMCs migration via interacting with MYH9 protein.

TPRG1-AS1 Affects F-Actin Stress Fiber Bundles Formation via Interacting With MYH9 Protein

The tails of MYH9 protein antiparallelly constitute bipolar filaments and bind with F-actin filaments to form stress fiber,[45] critical for control of cell shape and migration.[30] The overexpression of MYH9 gene in HASMCs could enhance stress fiber bundles formation, while the knockdown of MYH9 gene in HASMCs had an opposite

Figure 3 Continued. the targeted RNA levels enriched by TPRG1-AS1 probe, GAPDH, and LacZ Probe were used as negative control. **F**, Representative western blotting used to detect MYH9 protein retrieved by TPRG1-AS1 and control probes. **G**, Representative western blotting of the downregulation of MYH9 protein by the overexpression of TPRG1-AS1 in HASMCs. **H**, The statistical result in **G** (n=6 per group). **I**, Representative western blotting of the upregulation of MYH9 protein by the knockdown of TPRG1-AS1 in HASMCs. **J**, The statistical result in I (n=6 per group). **K**, Representative western blotting of MYH9 protein in HASMCs transfected with NC or siTPRG1-AS1 and treated with CHX (500 μM) for 0, 8, 16 hours. **L**, The statistical result in K (n=6 per group). **M**, Representative western blotting of MYH9 protein in HASMCs transfected with siNC or siTPRG1-AS1 and treated with MG132 (40 μM) for 24 hours. **N**, The statistical result in **L** (n=5 per group). Data were expressed as mean±SEM. Results in **D** are evaluated by paired *t* test. Results in **H** and **J** are evaluated by Student *t* test. Results in **L** are evaluated by 2-way ANOVA test. Results in **N** were performed using Brown-Forsythe and Welch ANOVA test followed by Dunn multiple comparison test.

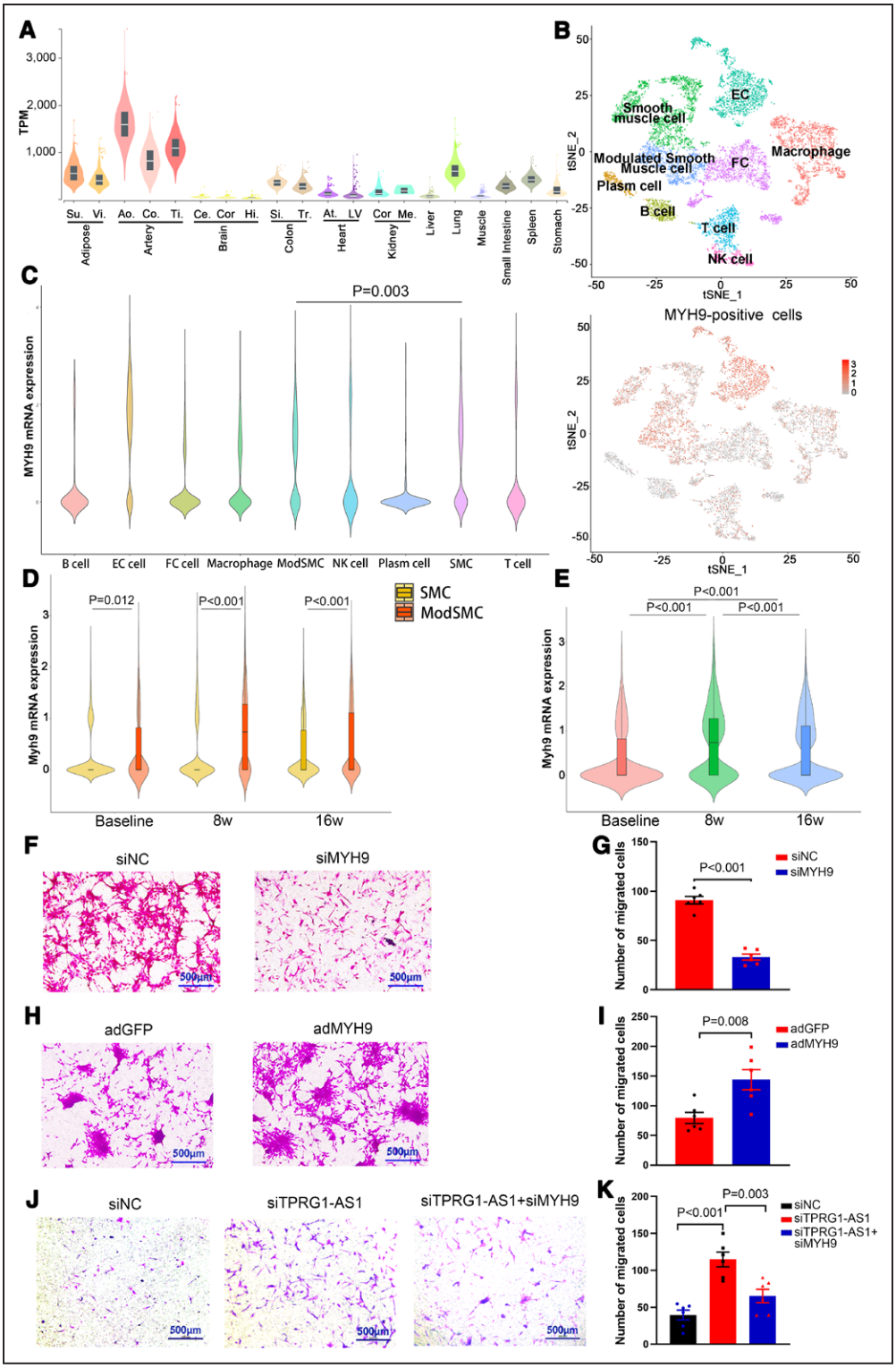

Figure 4. TPRG1-AS1 (tumor protein p63 regulated 1, antisense 1) inhibits human aortic smooth muscle cells (HASMCs) migration via interacting with MYH9 (myosin heavy chain 9) protein.

A, MYH9 expression across different human tissues in the GTEx database. **B**, t-SNE visualization of cell types and MYH9-postive cells in human atherosclerotic coronary artery (GSE131778). **C**, MYH9 mRNA expression levels in different cell types of human atherosclerotic coronary artery (GSE131778). ModSMC: phenotypically modulated SMCs. **D**, Myh9 mRNA expression levels in normal SMCs and ModSMC of *Apoe*$^{-/-}$ mice at baseline, 8 and 16 weeks of HFD feeding (GSE131776). **E**, Myh9 mRNA expression levels in ModSMC of *Apoe*$^{-/-}$ mice at baseline, 8 and 16 weeks of HFD feeding (GSE131776). **F**, Representative pictures of the effect of MYH9 gene knockdown on HASMCs migration. Scale bars, 500 μm. **G**, The statistical result in **F** (n=6 per group). **H**, Representative pictures of the effect of MYH9 gene overexpression on HASMCs migration. Scale bars, 500 μm. **I**, The statistical result in **H** (n=6 per group). (*Continued*)

effect (Figure 5A). We further investigated the effects of the interaction between TPRG1-AS1 with MYH9 protein on the stress fiber formation. The overexpression of TPRG1-AS1 could inhibit stress fiber formation in HASMCs treated with PDGF-BB (Figure 5B). However, the knockdown of TPRG1-AS1 in HASMCs promoted stress fiber bundles formation, which could be attenuated by the knockdown of MYH9 gene (Figure 5C), demonstrating that TPRG1-AS1 inhibited stress fiber bundles formation via interacting with MYH9 protein in HASMCs. Furthermore, Cytochalasin D (an actin depolymerizing agent[46]) treatment could significantly reverse not only increased stress fiber bundles (Figure 5D), but also increased HASMCs migration induced by the knockdown of TPRG1-AS1 (Figure 5E and 5F), indicating that the formation of stress fiber bundles was essential for increased HASMCs migration induced by the knockdown of TPRG1-AS1.

TPRG1-AS1 Overexpression Inhibits Neointima Formation In Vivo

Based on the results mentioned above, it was reasonable for us to evaluate the effects of TPRG1-AS1 on the vascular pathological response. To test this hypothesis, we examined the effects of the overexpression of TPRG1-AS1 on neointima formation in vivo induced by rat carotid balloon injury model. We first observed that the overexpression of TPRG1-AS1 significantly downregulated MYH9 protein in rat aortic smooth muscle cells (Figure S16A and S16B). Adenoviral vector (Ad-TPRG1-AS1 or Ad-GFP) was delivered to the injured left carotid artery. Two weeks after balloon injury, animals were euthanized, and the carotid arteries were fixed and embedded for histological analyses. Ad-TPRG1-AS1 significantly inhibited neointima formation, compared with Ad-GFP (Figure S16C). Such an inhibitory effect was associated with a decrease in both the intima area (Figure S16D) and the intima/media ratio (Figure S16E). These results confirmed that the overexpression of TPRG1-AS1 suppressed neointima formation in vivo.

To further validate the function of TPRG1-AS1 on vascular remodeling in vivo, we generated VSMC-specific TPRG1-AS1 transgenic mice (TPRG1-AS1^{SMCKI}). The primary mouse aortic smooth muscle cells of TPRG1-AS1^{SMCKI} and control mice were isolated, respectively. A high TPRG1-AS1 expression could be detected in MASMCs of transgenic mice, rather than control mice (Figure 6A; Figure S17). Consist with the decrease of MYH9 protein level in HASMCs transfected with Ad-TPRG1-AS1(Figure 3G and 3H), MYH9 protein level was significantly decreased in MASMCs of TPRG1-AS1^{SMCKI} mice, compared with control mice (Figure 6B and 6C) and there was also no significant difference in Myh9 mRNA levels between the 2 groups (Figure S18). Consistent with reduced F-actin stress fibers bundles and decreased migration of HASMCs transfected with Ad-TPRG1-AS1, MASMCs of TPRG1-AS1^{SMCKI} mice showed more disorganized and shortened actin stress fibers bundles and significantly decreased migration, compared with control mice (Figure 6D through 6F), further confirming that the interaction between TPRG1-AS1 and MYH9 protein inhibited stress fiber bundles formation and migration in MASMCs. Subsequently, we performed carotid artery wire injury in left common carotid artery of TPRG1-AS1^{SMCKI} mice and control mice. Two weeks after injury, TPRG1-AS1^{SMCKI} mice exhibited a drastic decrease in neointima formation compared with control mice (Figure 6G and 6H). However, the media of the injured carotid arteries did not differ between the groups. Therefore, the intima-to-media ratio was substantially lower in injured carotid arteries from TPRG1-AS1^{SMCKI} mice compared with control mice (Figure 6I). Collectively, these data demonstrated that VSMC-specific TPRG1-AS1 overexpression could inhibit wire injury-induced neointima formation in vivo.

VSMC-Specific TPRG1-AS1 Overexpression Attenuated Atherosclerosis

To further determine the role of VSMC-specific TPRG1-AS1 overexpression in the pathogenesis of atherosclerosis, we generated TPRG1-AS1^{SMCKI}*Apoe*$^{-/-}$ mice. At age 8 weeks, TPRG1-AS1^{SMCKI}*Apoe*$^{-/-}$ mice and control mice were fed with HFD for 20 weeks to establish atherosclerosis model. There were no significant differences in body weight, plasma total cholesterol and triglycerides between the 2 groups (Figure S20). Oil Red O staining showed that the en face-stained plaque area of TPRG1-AS1^{SMCKI}*Apoe*$^{-/-}$ mice was significantly reduced, compared with control mice (Figure 7A and 7B). H&E staining of aortic roots showed that the plaque area in aortic roots of TPRG1-AS1^{SMCKI}*Apoe*$^{-/-}$ mice was significantly decreased, compared with control mice (Figure 7C and 7D; Figure S21). Immunofluorescence staining of aortic roots showed that there was a significant reduction of MYH9-positive cells as percentage of plaque area in TPRG1-AS1^{SMCKI}*Apoe*$^{-/-}$ mice, compared with control mice (Figure 7E and

Figure 4 Continued. J, Representative pictures of the increase in HASMCs migration induced by the knockdown of TPRG1-AS1 was rescued by the knockdown of MYH9 gene. Scale bars, 500 μm. **K**, The statistical result of the rescue assay in **J** (n=6 per group). Results in **C**–**E** are evaluated by Wilcoxon rank-sum test. Data in **G**, **I**, and **K** were expressed as mean±SEM. Results in **G** and **I** are evaluated by Student *t* test. Results in **K** are evaluated by 1-way ANOVA followed by Tukey multiple comparison test. Ao indicates aorta; At, atrial appendage; Ce, cerebellum; Co, coronary; Cor, cortex; Hi, hippocampus; LV, left ventricle; Me, medulla; Si, Sigmoid; Su, subcutaneous; Ti, tibial; TPM, Transcripts Per kilobase Million; Tr, transverse; and Vi, visceral.

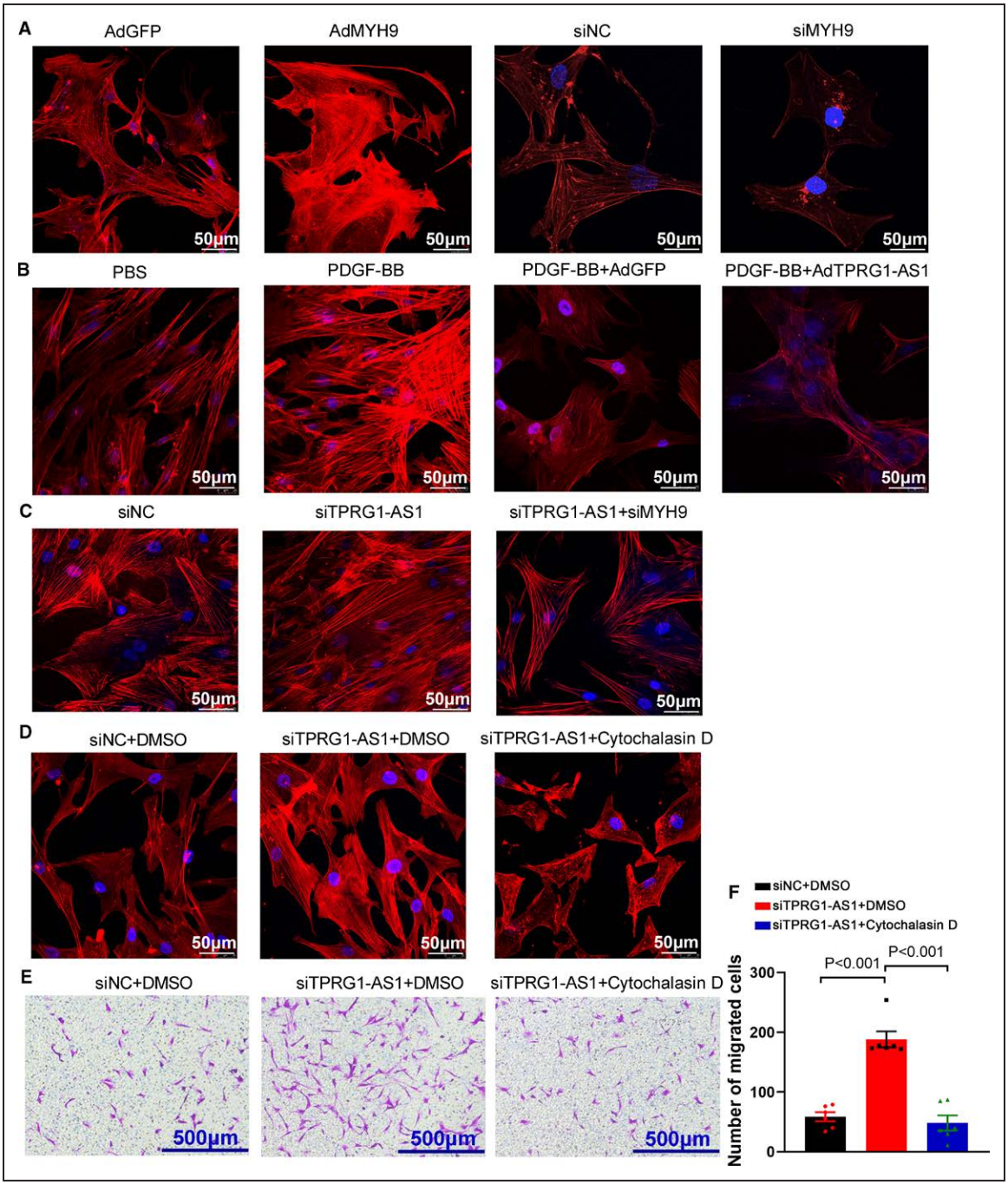

Figure 5. The interaction between TPRG1-AS1 (tumor protein p63 regulated 1, antisense 1) and MYH9 (myosin heavy chain 9) proteins affects stress fiber formation.

A, Representative pictures of the effect of the overexpression or knockdown of MYH9 gene on the stress fiber formation in human aortic smooth muscle cells (HASMCs). Scale bars, 50 μm. **B**, Representative pictures of the effect of the overexpression of TPRG1-AS1 on the stress fiber formation of HASMCs induced by PDGF-BB. Scale bars, 50 μm. **C**, Representative pictures of the increase of stress fiber information induced by the knockdown of TPRG1-AS1 was rescued by the knockdown of MYH9 gene. Scale bars, 50 μm. **D**, Representative pictures of the increase of stress fiber information induced by the knockdown of TPRG1-AS1 was rescued by the treatment of Cytochalasin D (30 μM, 24 hours). Scale bars, 50 μm. **E**, Representative pictures of the effect of Cytochalasin D (30 μM, 24 hours) on the increase in HASMCs migration induced by the knockdown of TPRG1-AS1. Scale bars, 500 μm. **F**, The statistical result in **E** (n=6 per group). Data were expressed as mean±SEM. Results in **F** are evaluated by 1-way ANOVA followed by Tukey multiple comparison test.

7F). These results demonstrated that VSMC-specific TPRG1-AS1 overexpression decreased MYH9 protein levels in atherosclerotic plaque and attenuated atherosclerotic lesions.

DISCUSSION

The abnormal migration of VSMCs from the media to the intima, contributing to neointima formation, is the

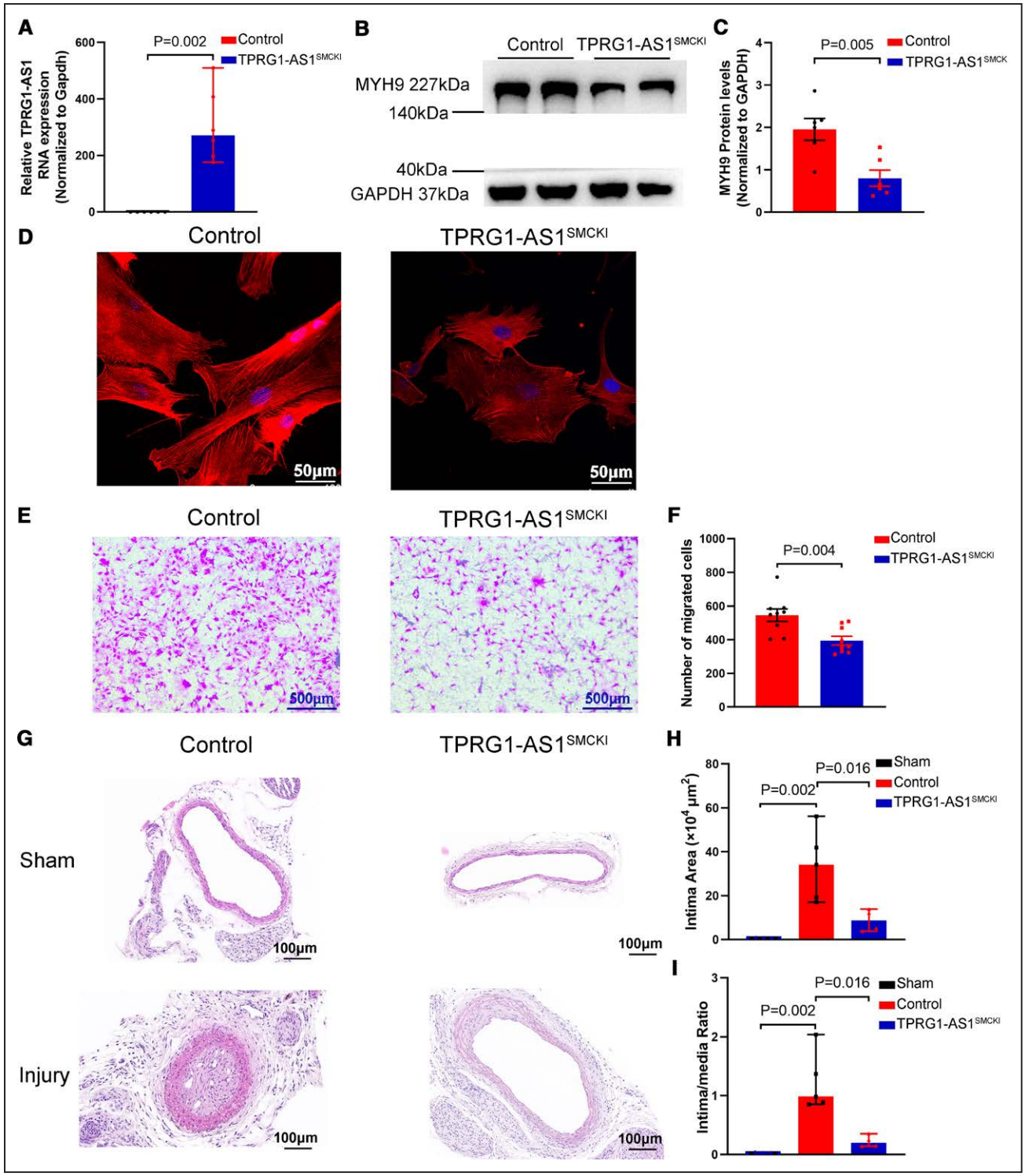

Figure 6. Vascular smooth muscle cell-specific TPRG1-AS1 (tumor protein p63 regulated 1, antisense 1) transgenic mice exhibit reduced neointima formation.

A, TPRG1-AS1 expression in murine aortic smooth muscle cells (MASMCs) isolated from TPRG1-AS1 transgenic mice were analyzed by qPCR (n=6 per group). **B**, Representative pictures of the MYH9 (myosin heavy chain 9) protein expression in MASMCs were analyzed by Western blot. **C**, The statistical result in **B** (n=6 per group). **D**, The effect of the overexpression of TPRG1-AS1 on the stress fiber formation of MASMCs. Scale bars, 50 μm. **E**, The effect of the overexpression of TPRG1-AS1 on MASMCs migration. Scale bars, 500 μm. **F**, The statistical result in E (n=9 per group). **G**, Representative hematoxylin-eosin-stained sections of the carotid arteries from TPRG1-AS1^{SMCKI} mice (n=4 mice), control mice (n=5 mice) 14 days after wire injury and sham littermates (n=5 mice). Scale bars, 100μm. **H**, Quantitative analysis of the intima area. (I) Quantitative analysis of intima/media ratio. Data in **A**, **H,** and **I** were expressed as median with 95% confidence limits. Data in **C** and **F** were expressed as mean±SEM. Results in **A** are evaluated by Mann-Whitney *U* test. Results in **C** and **F** are evaluated by Student *t* test. Results in **H** and **I** are evaluated by Kruskal-Wallis test.

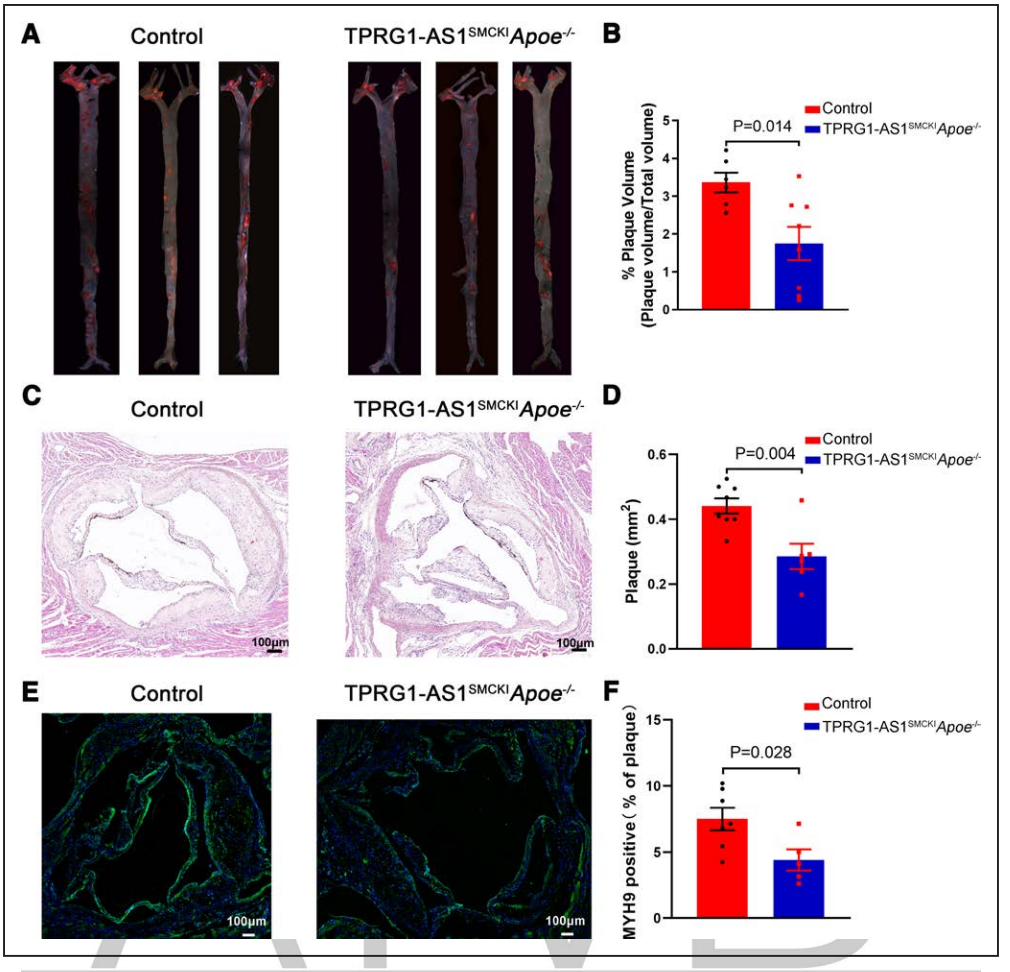

Figure 7. Vascular smooth muscle cell-specific TPRG1-AS1 (tumor protein p63 regulated 1, antisense 1) overexpression attenuated atherosclerosis.

A, Representative image for Oil Red O stained en face aorta of TPRG1-AS1^{SMCKI}*Apoe*$^{-/-}$ (n=8 mice) and control mice (n=6 mice) induced by HFD for 20 weeks. **B**, Quantitative assessment of plaque area in the whole aorta. **C**, Representative images for HE staining on aortic roots of TPRG1-AS1^{SMCKI} *Apoe*$^{-/-}$ mice (n=6 mice) and control mice (n=8 mice). Scale bars, 100 μm. **D**, Quantitative assessment of plaque area in the aortic root. **E**, Representative image for aortic roots that stained with an antibody against MYH9 (green). Scale bars, 100 μm. **F**, Percentage of MYH9 positive area (green) in atherosclerotic plaque of aortic root (n=5–6 mice per group). Data were expressed as mean±SEM. Results are evaluated by Student *t* test.

hallmark of atherosclerosis.[47] In our previous study, TPRG1-AS1 was identified as a novel lncRNA biomarkers for diagnosing CAD based on the transcriptome-wide lncRNA expression profile (GSE113079) of CAD patients and healthy controls,[20] but its role in the pathogenesis of CAD remains unknown. The present study focused on the role and underlying molecular mechanisms of lncRNA TPRG1-AS1 in the modulation of HASMCs migration, neointima formation, and atherosclerotic plaque formation.

The present study first analyzed the clinical relativity of TPRG1-AS1 with atherosclerosis, and the results from lncRNA/mRNA expression profile dataset (GSE97210)[27] and qRT-PCR detection in our own plaque samples showed that TPRG1-AS1 expression was significantly increased in atherosclerotic plaques, indicating the involvement of TPRG1-AS1 in the pathogenesis of atherosclerosis. Our study then characterized TPRG1-AS1 in HASMCs, including the size and the full length of TPRG1-AS1 transcript, and the subcellular location of endogenous TPRG1-AS1 in HASMCs, and finally identified TPRG1-AS1 as *bona fide* a lncRNA. Next, gain- and loss-of-function strategies were used to demonstrate that TPRG1-AS1 could regulate HASMCs migration rather than proliferation.[48]

Thus, it is of interest to further investigate the underlying mechanism of TPRG1-AS1 in regulating HASMC migration. Subcellular localization of TPRG1-AS1 in HASMCs indicated that TPRG1-AS1 might regulate HASMCs migration through physically interacting with proteins in cytoplasm, and MYH9 protein was screened and identified to interact with TPRG1-AS1 in HASMCs. Notably, the interaction between TPRG1-AS1 and MYH9 protein in HASMCs decreased MYH9 protein levels probably through the ubiquitin-proteasome pathway, but MYH9 mRNA levels were not significantly

changed. In nonmyocytes, MYH9 protein plays a critical role in cell adhesion and migration.[45] However, the role of MYH9 protein in HASMCs migration has not been fully recognized yet. According to the scRNA-seq datasets of human atherosclerotic plaques and aortic roots in *Apoe*$^{-/-}$ mice atherosclerosis model, MYH9 mRNA was significantly increased in phenotypically modulated SMCs compared with normal SMCs, indicating the involvement of MYH9 gene in SMC phenotyping switching, critical for the pathogenesis of atherosclerosis. To the best of our knowledge, the present study provided the first reported evidence that MYH9 gene could regulate HASMCs migration. Furthermore, the increased HASMCs migration induced by the knockdown of TPRG1-AS1 was reversed by the knockdown of MYH9 gene, demonstrating that the interaction between TPRG1-AS1 and MYH9 protein inhibited HASMCs migration.

Previous studies have reported that MYH9 proteins antiparallelly assemble into bipolar non-muscle myosin filaments that dynamically tether actin filaments to regulate stress fiber bundles formation and cell migration.[39,49,50] During smooth muscle cell migration, the dynamic reorganization of actomyosin cytoskeleton includes cell protrusion regulation, focal adhesion assembly/disassembly, and stress fiber formation.[51] A number of studies have shown that HASMCs migration requires actomyosin cytoskeleton reorganization.[51,52] For example, hypoxia inhibited HASMCs migration via inhibiting F-actin aggregation.[53] ARF GTPases were actively involved in the regulation of actin function in HASMCs migration, and ARF1 inhibition reduced HASMCs migration due to the inhibition of F-actin filaments.[54] MCP1 activated phosphorylation of cortactin on S405 and S418 residues in a time-dependent manner, and inhibition of its phosphorylation attenuated MCP1-induced HASMCs stress fiber formation and migration.[55] Therefore, we investigated the effects of the interaction between TPRG1-AS1 and MYH9 protein on stress fiber formation in HASMCs. The present study showed that the overexpression of MYH9 gene in HASMCs could promote the formation of stress fibers, while the knockdown of MYH9 gene in HASMCs had an opposite effect. The knockdown of MYH9 gene reversed the increased stress fiber formation induced by the knockdown of TPRG1-AS1, demonstrating that the interaction between TPRG1-AS1 and MYH9 protein inhibited stress fiber formation in HASMCs. Furthermore, the treatment of Cytochalasin D, an inhibitor of actin polymerization, could inhib not only stress fiber bundles formation but also HASMCs migration induced by the knockdown of TPRG1-AS1, demonstrating that the interaction between TPRG1-AS1 and MYH9 protein inhibited HASMCs migration through affecting stress fiber bundles formation. Similar to TPRG1-AS1, lncRNA MAFG-AS1 could directly bind to MYH9 protein, enhance the assembly of stress fiber in hepatoma cells, and promote cell migration.[33] Apart from that, several lncRNAs were also reported to affect cell migration by regulating the actomyosin cytoskeleton. For example, lncRNA EWSAT1 promoted cell migration and stress fiber bundles formation by acting a competing endogenous RNAs of ROCK1 through sponging miR-24-3p.[56] LINC00152 participated in F-actin reorganization, cytoskeletal remodeling, and regulated cell migration.[57] These findings suggested the important role of lncRNAs in the formation of stress fiber bundles and cell migration.

In order to confirm the results of experiments in vitro, rat carotid balloon injury model was used to evaluate the role of TPRG1-AS1 in neointima formation in vivo. The overexpression of TPRG1-AS1 in the injured left carotid artery could effectively reduce neointima formation in vivo. In addition to rat carotid balloon injury model, VSMC-specific *T*PRG1-AS1 transgenic mice was generated to further validate S Consistent with the results of TPRG1-AS1 overexpression in HASMCs, primary MASMCs isolated from VSMC-specific transgenic mice showed significant decrease in MYH9 protein levels with no significant difference in Myh9 mRNA levels and exhibited a reduction of stress fiber bundles formation and slower migration when compared with the control mice. Following, a well-established model of carotid artery wire injury was used to validate the function of TPRG1-AS1 in neointima formation in vivo. In line with the inhibition of HASMCs and MASMCs migration by TPRG1-AS1 in vitro, VSMC-specific overexpression of TPRG1-AS1 in transgenic mice significantly inhibited neointima formation in vivo. Thus, the above results validated protective role of TPRG1-AS1 overexpression in neointima formation in vivo.

Finally, functional consequence of the interaction between TPRG1-AS1 and MYH9 protein on HASMCs migration and the protective role of TPRG1-AS1 overexpression in neointima formation indicated that TPRG1-AS1 overexpression might attenuate atherosclerosis. Therefore, TPRG1-AS1^{SMCKI}*Apoe*$^{-/-}$ and control mice were fed with HFD for 20 weeks to establish an atherosclerosis model. By immunofluorescent staining, we observed that the percentage of MYH9-positive cells in plaque area were decreased in TPRG1-AS1^{SMCKI}-*Apoe*$^{-/-}$ mice compared with control mice, validating that VSMC-specific overexpression of TPRG1-AS1 could downregulate MYH9 protein in atherosclerotic plaque. The results of Oil red O and HE staining demonstrated that VSMC-specific TPRG1-AS1 overexpression had a protective effect on atherosclerotic plaque formation.

Generally, the high expression of lncRNA in atherosclerotic plaque is a sign of harmful effects, though with some exceptions. For instance, HO-1 was significantly upregulated in human vulnerable atherosclerotic lesions, but the overexpression of HO-1 inhibited vulnerable plaque development in *Apoe*$^{-/-}$ mice.[58] LncRNA RNCR3 was reported to be upregulated in atherosclerotic lesions compared with normal aortic tissues, but the knockdown

of RNCR3 in *Apoe*$^{-/-}$ mice aggregated atherosclerosis in vivo, indicating the protection role for the higher expression of RNCR3 in pathogenesis of atherosclerosis.[59] Although the expression of TPRG1-AS1 was significantly upregulated in atherosclerotic plaque, an atheroprotective effect of VSMC-specific overexpression of TPRG1-AS1 in *Apoe*$^{-/-}$ mice was observed in the present study. However, the upregulation of TPRG1-AS1 might have different functions at the different stage of atherosclerosis. In early stages of atherosclerosis, the migration of vascular smooth muscle cells from the media migrate into the intima promotes atherosclerotic plaque formation.[60] Moreover, vascular smooth muscle cells produce collagen to form a fibrous cap, which exerts a plaque stabilizing effect.[61] The inhibition of VSMCs migration could reduce atherosclerotic plaque formation at the early stage of plaque formation but lead to the thinning of fibrous cap and render plaque more unstable in the advanced plaque. As demonstrated in the present study, the overexpression of TPRG1-AS1 inhibited HASMCs migration, and VSMC-specific overexpression of TPRG1-AS1 attenuated atherosclerosis of *Apoe*$^{-/-}$mouse atherosclerosis model. However, TPRG1-AS1 expression was especially increased in advanced unstable atherosclerotic plaques (GSE97210),[27] and significantly increased in unstable region of atherosclerotic plaques compared with the stable region (GSE120521),[28] indicating the possible association of higher expression of TPRG1-AS1 in advanced plaque with plaque instability. Actually, unlike in human atherosclerotic lesion, spontaneous plaque rupture in *Apoe*$^{-/-}$ atherosclerotic mouse model is exceptionally rare and occurs only in aged mice (9-20 months).[62] In the present study, 8-week-old *Apoe*$^{-/-}$ mice were fed with HFD for only 20 weeks, therefore, a stronger inhibitory effect on plaque formation was observed. Hence, we speculated that the high expression of TPRG1-AS1 in advanced atherosclerotic plaque might lead to the thinning of fibrous cap and render plaque more unstable through inhibiting VSMCs migration, which needed to be validated using murine plaque rupture model in further work.

The scRNA-seq dataset of human atherosclerotic coronary arteries showed that MYH9 gene was widely expressed in multiple cell types of human atherosclerotic coronary arteries, and mainly expressed in smooth muscle cells and endothelial cells. Furthermore, the expression level of TPRG1-AS1 in different cells of human atherosclerotic coronary artery was not significantly different, though a relatively higher expression level of TPRG1-AS1 in HASMCs than in HUVECs confirmed by Northern blot. Given the critical role of HASMCs phenotype switching in the pathogenesis of atherosclerosis, the present study explored and confirmed the effect of TPRG1-AS1 on HASMCs migration. Consequently, we screened and identified intracellular binding proteins of TPRG1-AS1 in HASMCs via which TPRG1-AS1 regulated HASMCs migration. The interaction between TPRG1-AS1 and MYH9 protein might also exist in other cell types, which can be investigated in our future works.

In the present study, the interaction between TPRG1-AS1 and MYH9 protein resulted in degradation of MYH9 protein, and the exposure to the proteasome inhibitor MG132 resulted in increased MYH9 protein levels in HASMCs. Thus, we reasonably speculated that there might be a ribonucleic acid-protein complex composed of lncRNA TPRG1-AS1, MYH9 protein and yet unknown proteasome, and the binding of TRPG1-AS1 with MYH9 protein might promote the interaction between MYH9 protein and unkown proteasome, thus paving the way for the degradation of MYH9 protein. The identification of the ribonucleic acid-protein complex and underlying mechanism of degradation of MYH9 protein needed to be investigated in our future works.

Previous study indicated that there was no significant difference in MYH9 mRNA expression between human nonatherosclerotic artery and primary atherosclerotic lesions or restenotic atherosclerotic lesions.[63] Notably, the interaction between TPRG1-AS1 and MYH9 protein in HASMCs decreased MYH9 protein levels, but MYH9 mRNA levels were not significantly changed. In previous studies, there were no reports about the expression of MYH9 protein in human unstable and stable plaques. The relationship between TPRG1-AS1 and MYH9 protein in human unstable and stable plaques can be further explored in future works, verifying whether increased expression of TPRG1-AS1 results in decreased expression of MYH9 protein in human advanced plaques.

In addition to MYH9 protein, 4 other actin-binding proteins, namely NEXN,[64] profilin1,[65] Girdin,[66] and Drebrin,[67] were reported to be involved in neointima formation after vascular injury and the pathogenesis of atherosclerosis, respectively. Thus, accumulating evidence indicates that actin-binding proteins play critical roles in the pathogenesis of vascular pathological remodeling. The finding of the present study examining the F-actin-binding protein MYH9 provides evidence in this regard. However, the VSMC-specific Myh9 knockout mice should be used to further validate our results.

Since lncRNA TPRG1-AS1 inhibited HASMC migration and alleviated neointima formation and atherosclerosis in mice, a lncRNA TPRG1-AS1-based therapy could serve as a potential option for migrated VSMC-related occlusive vascular diseases. Zhang et al applied pH low-insertion peptide (pHLIP) as vehicles in atherosclerotic mice model, which provided proof of principle for the application of pHLIP as new delivery system for treating atherosclerosis.[68] Liu et al[69] utilized the biological functionality of neutrophil and the versatility of microbubble in the acoustic field to form Neu-balloon, which efficiently delivered drug into plaques in vivo. Xu et al[70] applied a multifunctional delivery nanosystem for targeting nucleic acid therapy of thoracic aortic dissection in mice model. These results provide insights into possibilities for ideal

approaches for transporting lncRNA TPRG1-AS1 to atherosclerotic plaque. However, before considering the application of TPRG1-AS1 in clinical practice, such as new delivery system-based coronary stent, the effect of new delivery systems should be evaluated in animal models first in our future works.

In summary, the present study illustrates anti-migratory function of TPRG1-AS1 in HASMCs in vitro and attenuation of VSMC-specific TPRG1-AS1 overexpression in neointima formation, and atherosclerosis in vivo and reveals underlying mechanism involving the interaction between TPRG1-AS1 and MYH9 protein, providing a novel insight and lncRNA-based potent inhibitor of HASMCs migration, potential therapies for migrated HASMCs-related occlusive vascular diseases.

ARTICLE INFORMATION

Received March 17, 2022; accepted September 14, 2022.

Affiliations

Key Laboratory of Cardiovascular Epidemiology and Department of Epidemiology, State Key Laboratory of Cardiovascular Disease (X.R., H.Z., K.D., X.N., D.L., B.Y., S.C., D.G., L.W.), Department of Vascular Surgery, State Key Laboratory of Cardiovascular Disease (C.S.), Department of Surgery (X.W.), and Cardiometabolic Center (N.W.), Fuwai Hospital, National Center for Cardiovascular Diseases, Chinese Academy of Medical Sciences and Peking Union Medical College, Beijing, China.

Acknowledgments

D. Gu and L. Wang conceived and supervised the research. H. Zhu, X. Ning, and L. Li performed molecular and cellular experiments and analyzed the data. X. Ren, K. Deng, and D. Liu performed animal experiments and analyzed the data. X. Ren, H. Zhu, and L. Wang wrote the article. C. Shen, X. Wang, N. Wu, B. Yang, and S. Chen reviewed and edited the article.

Sources of Funding

This work was supported by the Natural Science Foundation of Beijing (No.7212081); the National Natural Science Foundation of China (No. 82170480, 82030102); CAMS Innovation Fund for Medical Sciences (CIFMS; No.2016-I2M-1-009).

Disclosures

None.

Supplemental Material

Major Resources Table
Figures S1–S21
Tables S1–S9

REFERENCES

1. Zhao TM. Targeting the immune system in atherosclerosis: Jacc state-of-the-art review. *J Am Coll Cardiol*. 2019;73:1691–1706. doi: 10.1016/j.jacc.2018.12.083
2. Nadiya Khyzha AA, Michael D. Wilson, Jason E. Fish. Epigenetics of atherosclerosis: Emerging mechanisms and methods. *Trends Mol Med*. 2017;23:332–347. doi: 10.1016/j.molmed.2017.02.004
3. Baumgartner IS, Graziani L. Management of peripheral vascular disease. *Annu Rev Med*. 2005;56:249–272.
4. Virani SS, Alonso A, Aparicio HJ, Benjamin EJ, Bittencourt MS, Callaway CW, Carson AP, Chamberlain AM, Cheng S, Delling FN. et al. Heart disease and stroke statistics-2021 update: a report from the american heart association. *Circulation*. 2021;143:e254–e743. doi: 10.1161/CIR.0000000000000950
5. Basatemur GJ, Clarke MCH, Bennett MR, Mallat Z. Vascular smooth muscle cells in atherosclerosis. *Nat Rev Cardiol*. 2019;16:727–744.
6. Gomez D, Owens GK. Smooth muscle cell phenotypic switching in atherosclerosis. *Cardiovasc Res*. 2012;95:156–164. doi: 10.1093/cvr/cvs115
7. Jukema JW, Verschuren JJ, Ahmed TA, Quax PH. Restenosis after pci. Part 1: pathophysiology and risk factors. *Nat Rev Cardiol*. 2011;9:53–62. doi: 10.1038/nrcardio.2011.132
8. Chen LJ, Lim SH, Yeh YT, Lien SC, Chiu JJ. Roles of micrornas in atherosclerosis and restenosis. *J Biomed Sci*. 2012;19:79. doi: 10.1186/1423-0127-19-79
9. Owens GK, Kumar MS, Wamhoff BR. Molecular regulation of vascular smooth muscle cell differentiation in development and disease. *Physiol Rev*. 2004;84:767–801. doi: 10.1152/physrev.00041.2003
10. Raines EW, Ross R. Smooth muscle cells and the pathogenesis of the lesions of atherosclerosis. *Br Heart J*. 1993;69:S30–S37. doi: 10.1136/hrt.69.1_suppl.s30
11. Zhu JF, Wu Y, Zheng X. Function of lncrnas and approaches to lncrna-protein interactions. *Sci China Life Sci*. 2013;56:876–885. doi: 10.1007/s11427-013-4553-6
12. Zhang YZ, Xu BM, Tang WH, et al. Lncrna-rp11-714g18.1 suppresses vascular cell migration via directly targeting lrp2bp. *Immunol Cell Biol*. 2018;96:175–189. doi: 10.1111/imcb.1028
13. Archer KB, Bayoumi AS, Teoh JP, Davila A, Tang Y, Su H, Kim IM. Long noncoding rnas as master regulators in cardiovascular diseases. *Int J Mol Sci*. 2015;16:23651–23667. doi: 10.3390/ijms161023651
14. Liu YZ, Wang Q, Hu YW. Emerging roles and mechanisms of long noncoding rnas in atherosclerosis. *Int J Cardiol*. 2017;228:570–582. doi: 10.1016/j.ijcard.2016.11.182
15. Mazidi MP, Gluba-Brzozka A, Rysz J, Banach M. Relationship between long noncoding rnas and physiological risk factors of cardiovascular disease. *J Clin Lipidol*. 2017;11:617–623. doi: 10.1016/j.jacl.2017.03.009
16. Wang ZZ, Ji YX, Zhang P, et al. The long noncoding rna chaer defines an epigenetic checkpoint in cardiac hypertrophy. *Nat Med*. 2016;22:1131–1139. doi: 10.1038/nm.4179.
17. Jin L, Lin X, Yang L, Fan X, Wang W, Li S, Li J, Liu X, Bao M, Cui X. et al. Ak098656, a novel vascular smooth muscle cell-dominant long noncoding rna, promotes hypertension. *Hypertension*. 2018;71:262–272. doi: 10.1161/HYPERTENSIONAHA.117.09651
18. Chengxin Zhang SG, Wenhui G, Jinguo X, Zhixiang G, Zhuang L, Xiaotian G, Xiaoyong W, Shenglin G. LncRNA ANRIL acts as a modular scaffold of WDR5 and HDAC3 complexes and promotes alteration of the vascular smooth muscle cell phenotype. *Cell Death Dis*. 2020;11:435. doi: 10.1038/s41419-020-2645-3
19. Dong K, Shen J, He X, et al. Carmn is an evolutionarily conserved smooth muscle cell-specific lncrna that maintains contractile phenotype by binding myocardin. *Circulation*. 1856;202:1875.
20. Li L, Wang L, Li H, Han X, Chen S, Yang B, Hu Z, Zhu H, Cai C, Chen J. et al. Characterization of lncrna expression profile and identification of novel lncrna biomarkers to diagnose coronary artery disease. *Atherosclerosis*. 2018;275:359–367. doi: 10.1016/j.atherosclerosis.2018.06.866
21. Robinet P, Milewicz DM, Cassis LA, Leeper NJ, Lu HS, Smith JD. Consideration of sex differences in design and reporting of experimental arterial pathology studies-statement from atvb council. *Arterioscler Thromb Vasc Biol*. 2018;38:292–303. doi: 10.1161/ATVBAHA.117.309524
22. Nofer JR. Estrogens and atherosclerosis: Insights from animal models and cell systems. *J Mol Endocrinol*. 2012;48:R13–R29. doi: 10.1530/JME-11-0145
23. Watanabe T, Miyahara Y, Akishita M, Nakaoka T, Yamashita N, Iijima K, Kim H, Kozaki K, Ouchi Y. Inhibitory effect of low-dose estrogen on neointimal formation after balloon injury of rat carotid artery. *Eur J Pharmacol*. 2004;502:265–270. doi: 10.1016/j.ejphar.2004.09.011
24. Daugherty A, Tall AR, Daemen M, et al. Recommendation on design, execution, and reporting of animal atherosclerosis studies: A scientific statement from the american heart association. *Arterioscler Thromb Vasc Biol*. 2017;37:e131–e157. doi: 10.1161/ATV.0000000000000062
25. Li J, Liu X, Tan L, Cui Z, Yang X, Liang Y, Li Z, Zhu S, Zheng Y, Yeung KWK. et al. Zinc-doped prussian blue enhances photothermal clearance of staphylococcus aureus and promotes tissue repair in infected wounds. *Nat Commun*. 2019;10:4490. doi: 10.1038/s41467-019-12429-6
26. Consortium GT, Laboratory DA, Coordinating Center -Analysis Working G, Statistical Methods groups-Analysis Working G, Enhancing Gg, Fund NIHC, et al. Genetic effects on gene expression across human tissues. *Nature*. 2017;550:204–213. doi: 10.1038/nature24277
27. Bai HL, Lu ZF, Zhao JJ, Ma X, Li X-H, Xu H, Wu S-G, Kang C-M, Lu J-B, Xu Y-J. et al. Microarray profiling analysis and validation of novel long noncoding rnas and mrnas as potential biomarkers and their functions in atherosclerosis. *Physiol Genomics*. 2019;51:644–656. doi: 10.1152/physiolgenomics.00077.2019

28. Mahmoud AD, Ballantyne MD, Miscianinov V, Pinel K, Hung J, Scanlon JP, Iyinikkel J, Kaczynski J, Tavares AS, Bradshaw AC. et al. The human-specific and smooth muscle cell-enriched lncrna smilr promotes proliferation by regulating mitotic cenpf mrna and drives cell-cycle progression which can be targeted to limit vascular remodeling. *Circ Res*. 2019;125:535–551. doi: 10.1161/CIRCRESAHA.119.314876
29. Wirka RC, Wagh D, Paik DT, Pjanic M, Nguyen T, Miller CL, Kundu R, Nagao M, Coller J, Koyano TK. et al. Atheroprotective roles of smooth muscle cell phenotypic modulation and the tcf21 disease gene as revealed by single-cell analysis. *Nat Med*. 2019;25:1280–1289. doi: 10.1038/s41591-019-0512-5
30. Lee S, Kopp F, Chang TC, Sataluri A, Chen B, Sivakumar S, Yu H, Xie Y, Mendell JT. Noncoding rna norad regulates genomic stability by sequestering pumilio proteins. *Cell*. 2016;164:69–80. doi: 10.1016/j.cell.2015.12.017
31. Wu M, Yang LZ, Chen LL. Long noncoding rna and protein abundance in lncrnps. *RNA*. 2021;27:1427–1440. doi: 10.1261/rna.078971.121
32. Holycross BJ1 BR, Thompson MM, Peach MJ, Owens GK. Platelet-derived growth factor-bb-induced suppression of smooth muscle cell differentiation. *Circ Res*. 1992;71:1525–1532. doi: 10.1161/01.res.71.6.1525
33. Zhang F, Li Y, Gan L, Tong X, Qi D, Wang Q, Ye X. Hbx-upregulated mafg-as1 promotes cell proliferation and migration of hepatoma cells by enhancing mafg expression and stabilizing nonmuscle myosin iia. *FASEB J*. 2021;35:e21529. doi: 10.1096/fj.202002374R
34. Sun J, Guo Y, Chen T, Jin T, Ma L, Ai L, Guo J, Niu Z, Yang R, Wang Q. et al. Systematic analyses identify the anti-fibrotic role of lncrna tp53tg1 in ipf. *Cell Death Dis*. 2022;13:525. doi: 10.1038/s41419-022-04975-7
35. Deng C, Zhang B, Zhang Y, Xu X, Xiong D, Chen X, Wu J. A long non-coding rna olbc15 promotes triple-negative breast cancer progression via enhancing znf326 degradation. *J Clin Lab Anal*. 2020;34:e23304. doi: 10.1002/jcla.23304
36. Li Y, Wang Z, Su P, Liang Y, Li Z, Zhang H, Song X, Han D, Wang X, Liu Y. et al. Circ-eif6 encodes eif6-224aa to promote tnbc progression via stabilizing myh9 and activating the wnt/beta-catenin pathway. *Mol Ther*. 2022;30:415–430. doi: 10.1016/j.ymthe.2021.08.026
37. Chen W, Wang W, Sun X, Xie S, Xu X, Liu M, Yang C, Li M, Zhang W, Liu W. et al. Nudcl2 regulates cell migration by stabilizing both myosin-9 and lis1 with hsp90. *Cell Death Dis*. 2020;11:534. doi: 10.1038/s41419-020-02739-9
38. Asensio-Juarez G, Llorente-Gonzalez C, Vicente-Manzanares M. Linking the landscape of myh9-related diseases to the molecular mechanisms that control non-muscle myosin ii-a function in cells. *Cells*. 2020;9:1458. doi: 10.3390/cells9061458
39. Vicente-Manzanares M, Ma X, Adelstein RS, Horwitz AR. Non-muscle myosin ii takes centre stage in cell adhesion and migration. *Nat Rev Mol Cell Biol*. 2009;10:778–790. doi: 10.1038/nrm2786
40. Morin NO, Hyun YM, Lee D, Chin YE, King MR, Springer TA, Shimaoka M, Tang JX, Reichner JS, Kim M. Nonmuscle myosin heavy chain iia mediates integrin lfa-1 de-adhesion during t lymphocyte migration. *J Exp Med*. 2008;205:195–205. doi: 10.1084/jem.20071543
41. Huang YS, Zhou H, Song X, Yuan S, Luo Y. The angiogenic function of nucleolin is mediated by vascular endothelial growth factor and nonmuscle myosin. *Blood*. 2006;107:3564–3567. doi: 10.1182/blood-2005-07-2961
42. Vicente-Manzanares MM, Adelstein RS, Horwitz AR. Non-muscle myosin ii takes centre stage in cell adhesion and migration. *Nat Rev Mol Cell Biol*. 2009;10:778–790. doi: 10.1038/nrm2786
43. Sajid M, Hu Z, Lele M, Stouffer GA. Protein complexes involving alpha v beta 3 integrins, nonmuscle myosin heavy chain-a, and focal adhesion kinase from in thrombospondin-treated smooth muscle cells. *J Investig Med*. 2000;48:190–197.
44. Gallagher PJ, Jin Y, Killough G, Blue EK, Lindner V. Alterations in expression of myosin and myosin light chain kinases in response to vascular injury. *Am J Physiol Cell Physiol*. 2000;279:C1078–C1087. doi: 10.1152/ajpcell.2000.279.4.C1078
45. Brito C, Sousa S. Non-muscle myosin 2a (nm2a): Structure, regulation and function. *Cells*. 2020;9;1590. doi: 10.3390/cells9071590
46. Suzuki JJ, Meoli DF, Matoba T, Berk BC. Cyclophilin a is secreted by a vesicular pathway in vascular smooth muscle cells. *Circ Res*. 2006;98:811–817. doi: 10.1161/01.RES.0000216405.85080.a6
47. Libby P. Inflammation in atherosclerosis. *Nature*. 2002;420:868–874.
48. Hulin-Curtis S, Williams H, Wadey KS, Sala-Newby GB, George SJ. Targeting wnt/beta-catenin activated cells with dominant-negative n-cadherin to reduce neointima formation. *Mol Ther Methods Clin Dev*. 2017;5:191–199. doi: 10.1016/j.omtm.2017.04.009
49. Cao Y, Lei Y, Luo Y, et al. The actomyosin network is influenced by nmhc iia and regulated by crp(f46), which is involved in controlling cell migration. *Exp Cell Res*. 2018;373:119–131. doi: 10.1016/j.yexcr.2018.10.004
50. Agarwal P, Zaidel-Bar R. Diverse roles of non-muscle myosin ii contractility in 3d cell migration. *Essays Biochem*. 2019;63:497–508. doi: 10.1042/EBC20190026
51. Tang DD. The dynamic actin cytoskeleton in smooth muscle. *Adv Pharmacol*. 2018;81:1–38. doi: 10.1016/bs.apha.2017.06.001
52. WT G. Mechanisms of vascular smooth muscle cell migration. *Circ Res*. 2007;100:607–621. doi: 10.1161/01.RES.0000258492.96097.47
53. Yang M, Fan Z, Wang F, et al. Bmp-2 enhances the migration and proliferation of hypoxia-induced vsmcs via actin cytoskeleton, cd44 and matrix metalloproteinase linkage. *Exp Cell Res*. 2018;368:248–257. doi: 10.1016/j.yexcr.2018.05.004
54. Charles RB, Claing A. Arf gtpases control phenotypic switching of vascular smooth muscle cells through the regulation of actin function and actin dependent gene expression. *Cell Signal*. 2018;46:64–75. doi: 10.1016/j.cellsig.2018.02.012
55. Janjanam JC, Kotla S, Rao GN. Plcβ3 mediates cortactin interaction with wave2 in mcp1-induced actin polymerization and cell migration. *Mol Biol Cell*. 2015;26:4589–4606. doi: 10.1091/mbc.E15-08-0570
56. Shen D, Liu Y, Liu Y, et al. Long non-coding rna ewsat1 promoted metastasis and actin cytoskeleton changes via mir-24-3p sponging in osteosarcoma. *J Cell Mol Med*. 2021;25:716–728. doi: 10.1111/jcmm.16121
57. Tang Y, He Y, Zhang P, et al. Lncrnas regulate the cytoskeleton and related rho/rock signaling in cancer metastasis. *Mol Cancer*. 2018;17:77. doi: 10.1186/s12943-018-0825-x
58. Cheng C, Noordeloos AM, Jeney V, et al. Heme oxygenase 1 determines atherosclerotic lesion progression into a vulnerable plaque. *Circulation*. 2009;119:3017–3027. doi: 10.1161/CIRCULATIONAHA.108.808618
59. Shan K, Jiang Q, Wang XQ, et al. Role of long non-coding rna-rncr3 in atherosclerosis-related vascular dysfunction. *Cell Death Dis*. 2016;7:e2248. doi: 10.1038/cddis.2016.145
60. Doran AC, Meller N, McNamara CA. Role of smooth muscle cells in the initiation and early progression of atherosclerosis. *Arterioscler Thromb Vasc Biol*. 2008;28:812–819. doi: 10.1161/ATVBAHA.107.159327
61. Newby AC, Zaltsman AB. Fibrous cap formation or destruction--the critical importance of vascular smooth muscle cell proliferation, migration and matrix formation. *Cardiovasc Res*. 1999;41:345–360.
62. Calara F, Silvestre M, Casanada F, Yuan N, Napoli C, Palinski W. Spontaneous plaque rupture and secondary thrombosis in apolipoprotein e-deficient and ldl receptor-deficient mice. *J Pathol*. 2001;195:257–263. doi: 10.1002/path.915
63. Nikol S, Murakami N, Pickering JG, et al. Differential expression of non-muscle myosin ii isoforms in human atherosclerotic plaque. *Atherosclerosis*. 1997;130:71–85. doi: 10.1016/s0021-9150(96)06047-9
64. Hu YG, Xu YJ, Li P, et al. Long noncoding rna nexn-as1 mitigates atherosclerosis by regulating the actin-binding protein nexn. *J Clin Invest*. 2019;129:1115–1128. doi: 10.1172/JCI98230
65. Romeo GM, Kazlauskas A. Attenuated expression of profilin-1 confers protection from atherosclerosis in the ldl receptor null mouse. *Circ Res*. 2007;101:357–367. doi: 10.1161/CIRCRESAHA.107.151399
66. Miyake HM, Asai N, Shibata R, Ichimiya H, Isotani-Sakakibara M, Yamamura Y, Kato K, Enomoto A, Takahashi M, Murohara T. The actin-binding protein girdin and its akt-mediated phosphorylation regulate neointima formation after vascular injury. *Circ Res*. 2011;108:1170–1179. doi: 10.1161/CIRCRESAHA.110.236174
67. Stiber JW, Zhang L, Nepliouev I, Zhang ZS, Bryson VG, Brian L, Bentley RC, Gordon-Weeks PR, Rosenberg PB, Freedman NJ. The actin-binding protein drebrin inhibits neointimal hyperplasia. *Arterioscler Thromb Vasc Biol*. 2016;36:984–993. doi: 10.1161/ATVBAHA.115.306140
68. Zhang X, Rotllan N, Canfran-Duque A, et al. Targeted suppression of mirna-33 using phlip improves atherosclerosis regression. *Circ Res*. 2022;131:77–90. doi: 10.1161/CIRCRESAHA.121.320296
69. Liu F, Mao Y, Yan J, et al. Bionic microbubble neutrophil composite for inflammation-responsive atherosclerotic vulnerable plaque pluripotent intervention. *Research (Wash D C)* 2022;9830627. doi: 10.34133/2022/9830627
70. Xu C, Zhang Y, Xu K, et al. Multifunctional cationic nanosystems for nucleic acid therapy of thoracic aortic dissection. *Nat Commun*. 2019;10:3184. doi: 10.1038/s41467-019-11068-1